

Graduation Thesis

Predictive Wildfire Damage to Populated Regions at Wildland-Urban Interfaces:
A Case-Based Survey of Risk Factors in Victoria, Australia and
California, United States

July 2019

Department of Interdisciplinary Sciences

International Program on Environmental Sciences

The University of Tokyo

Alexander Zen Taniguchi (Wiegman)

Abstract

Predictive Wildfire Damage to Populated Regions at Wildland-Urban Interfaces: A Case-Based Survey of Risk Factors in Victoria, Australia and California, United States

Department of Interdisciplinary Sciences

International Program on Environmental Sciences

The University of Tokyo

Alexander Zen Taniguchi (Wiegman)

With our rising populations and urban sprawl, contemporary urban planning requires consideration of problems that were previously studied primarily in uninhabited regions. Among these issues is the exposure to the risk of wildfires affecting human lives and infrastructure security. Existing research to detect fires and burned land has looked at nighttime lights and thermal satellites' imagery in the United States, detailed visible-light imagery in Australia, and atmospheric particulate matter imagery in Thailand. Further, disaster management policymakers mitigate wildfire hazards by discussing road planning, improving emergency response times, and holding general awareness campaigns to inform the public. As a part of that awareness program, these regions publish Fire Hazard Maps, showing historical data on fire occurrences and current situations on potentially hazardous factors including wind, soil dryness, fire fuel types, and air temperature. However, most data used to construct these maps were outdated by over ten years, and the above regions have yet to publish a predictive map which considers future urban sprawl. To this end, this research selected a significant wildfire case in each of California (Camp Fire, 2018) and Victoria (Black Saturday Fires, 2009), based on impact to human life and property damage. Google Earth Engine was used to visualize the below data, because of its efficiency for combining separate GIS datasets across a wide spatiotemporal variance.

This investigation obtained fire hazard data from Fire Information for Resource Management System (FIRMS) and Moderate Resolution Imaging Spectroradiometer (MODIS) Category 6 Burned Area Product, Landsat passive sensor surface-reflectance imagery, and (where available) Sentinel active sensor surface-reflectance imagery. Current and historical land-usage was determined by the supervised classification of Landsat images using aerial imagery in Google Earth. The predictive land-usage analysis was computed within a python-scripted Cellular Automata-Artificial Neural Network (CA-ANN) machine learning tool “Modules for Land Use Change Simulations (MOLUSCE),” using the already known land-usage analysis data from Landsat and Google Earth Engine. More exposure variables were evaluated using population maps from WorldPop, nighttime lighting population indications from Visible Infrared Imaging Radiometer Suite (VIIRS), and Defense Meteorological Program Operational Line-Scan System (DMSP-OLS) products. Potential drought vulnerability information was evaluated using soil moisture and temperature maps from Global Land Data Assimilation System (GLDAS), wind direction maps from Real-Time Mesoscale Analysis (RTMA) and Gridded Surface Meteorological Dataset (GRIDMET), and precipitation maps from Global Satellite Mapping of Precipitation (GSMaP). This study also mapped locations of fire stations from Google Earth to showcase potential social vulnerability. These factors, as currently known in 2019, were all exported onto multiple distinct maps for predicted urbanization in 2030 and 2040 to create predictive fire hazard maps. They were placed alongside similar fire hazard maps for 2000 and 2010 to give validation to the methodology.

Findings from Victoria showed that it was reasonable to believe that a city could rebuild urban areas lost to fire within ten years. That said, this study did not anticipate the severe drop in population density over spatial proximities, both in the historical and predictive timescales – each of the cities selected for loss-to-fire analysis was significantly less densely populated than the metropolitan cities present within a 50km radius. However, the study of wind-directionality and real-time flame progression during the fires showed progress in the direction of these major cities, and the Victoria Black Saturday Fires especially showed that some flames reached the outer Melbourne District (the capital city of the state of Victoria). In addition to the cultural limitation of population density, Australia’s wind direction data was underrepresented: data was not available to be mapped or visualized at a similar resolution to other products. While these shortcomings exist, the presentation of this and comparable data to policymakers and citizen science groups may allow for awareness and brainstorming to mitigate similar hazards in any city across Earth. This research study, willing to aid anyone who wishes to undertake such efforts, has made available the Predictive Fire Hazard Maps and its associated programming code on the publicly-open platform “GitHub” and within a “Google Earth Engine App.”

Acknowledgments

Many thanks to my advisor, Dr. Wataru Takeuchi of Institute of Industrial Sciences at the University of Tokyo, for his guidance and supervision. Many others also helped in the creation of this thesis. I want to start by thanking a couple of post-docs of our laboratory, Dr. Haemi Park and Dr. Prakhar Mishra, for their expertise and comments which helped clarify the presentation of ideas in both this paper and its associated defense presentation. Next, Mr. Truong Trinh Xuan for his help in making sure that this study follows a plan – both in terms of organizing the ideas and timetable, which led to its timely completion. The Google Earth Japan and Mountain View teams – with distinction to Mr. Michael DeWitt and Dr. Nicholas Clinton – made this study possible through their work in developing the Google Earth Engine product and in training users how to make practical visualization tools. Also, to Ms. M. van der Braak, MSc and other anonymous proofreaders for their invaluable suggestions after proofreading this study’s manuscripts. Finally, with thanks to the many other members of the W. Takeuchi laboratory family who have given constructive criticism, suggested potential areas of focus, lent a listening ear to ideas, consoled worries with jokes and laughter, and made sure I ate by cooking dishes from around the world or bringing snacks. It will be a bitter parting with the laboratory family upon graduation, but I will never forget everyone’s kindness. Hopefully, like the few students before, the many more after will also experience the joy of being in such a lively family of researchers.

Dedications

I dedicate this work to the victims of each of these fires – who lost their property, their livelihoods, and sometimes their lives. Their stories are a necessary premise for conducting this research, and I wish there to be fewer such disasters in our future.

Also, to my family, for their support through a decision to attend University very far away from where they live. While a challenge at first, the impact this decision has had since is quite significant. Without them, it is quite likely I would have never made it this far into my bachelor's degree study.

Table of Contents

Section	Page #
Abstract	ii – iii
Acknowledgments	iv
Dedications	v
Table of Contents	vi
List of Tables	vii
List of Figures	viii – ix
Section 1. Introduction	1 – 5
Section 2. Methodology	6 – 23
Section 3. Results and Discussion	24 – 41
Section 4. Conclusion and Future Work	42 – 44
Appendix A. Communication of Data with the Public	45 – 47
References	48 – 51

List of Tables

Table Number and Description	Page #
1. Location, Climate, and Death Toll of the Top 20 Deadliest Fires on Record (for 2000 - mid-2019)	6
2. Timescale: Years for which Satellite Imagery Collection was Collected in Each Study Region	8
3. Satellite Products Used, provided through Google Earth Engine	10
4. Number of Polygons Drawn as Classification Samples for the “Normal” and “Burnt” Datasets of Case-Study Wildfires	13
5. In Which Years DMSP-OLS and VIIRS Images were Downloaded for each Case-Study Wildfire	18
6. Color Assigned to Each Landcover Classification (with Sample)	29
7. Satellite-Dependent Landcover Simulation’s Validation (in Percentage of Accuracy), for each Case-Study WUI Region	33
8. Fire Response Time Standards, Lawful Maximum Driving Speed, and Effective Response-Ready Area for each Study Area	41

List of Figures

Figure Number and Description	Page #
1. Remote Sensing vs. Classical Data Collection	2
2. Regions of Study in Northern California for Camp Fire, 2018	7
3. Regions of Study in Southern Victoria for Black Saturday Fires, 2009	7
4. The rectangular boundary for the Camp Fire’s Region of Interest in northern California	9
5. The rectangular boundary for the Black Saturday Fire’s Region of Interest in southern Victoria	9
6. A Sample of Each Classification Type.	12
7. An example of a “KEEP CLEAR” sign at a South Morang, Victoria fire station.	13
8. Flowchart of steps used to study Hazard Factors	14
9. dNBR thresholds for each level of burn severity	15
10. Flowchart of Steps used to study Exposure Factors	16
11. Generalized depiction of a model Artificial Neural Network (ANN).	19
12. Flowchart of Steps used to study Vulnerability Factors	21
13. Camp Fire wildfire spread, esp. near WUI communities	24
14. Black Saturday Fires wildfire spread, esp. near WUI communities	25
15. Camp Fire burned area polygon measured with ruler in Google Earth	26
16. Black Saturday Fires burned area polygon measured with ruler in Google Earth	26
17. Burn severity and locations of surrounding area maps	27
18. Spectra graphs of Landsat 8 Surface Reflectance (SR) in Paradise, California	28
19. Landcover change in Camp Fire study area from 2000 – 2018	30
20. Landcover change in Black Saturday Fires study area from 2000 – 2018	30
21. WorldPop population density of Camp Fire study area	31
22. WorldPop population density of Black Saturday Fires study area	31
23. Proxy Population by NTL Change in Camp Fire study area	32
24. Proxy Population by NTL Change in Camp Fire study area	32
25. “Real” vs. “Simulated” image in California, comparing classification accuracy	34

Figure Number and Description (Continued)	Page #
26. “Real” vs. “Simulated” image in Victoria, comparing classification accuracy	34
27. Result of Simulation predicting landcover classes for (the year) 2030	34
28. Result of Simulation predicting landcover classes for (the year) 2040	35
29. Urban Densification & Creation in the Camp Fires’ Zone of Exposure	35
30. Urban Densification & Creation in the Black Saturday Fires’ Zone of Exposure	35
31. Per-decade comparison of temperature in California and Victoria, 2000- 2018	36
32. Per-decade comparison of soil moisture in California and Victoria, 2000- 2018	37
33. Comparison of wind direction and fire progression for the first day of each fire	38
34. Per-decade comparison of rainfall in California and Victoria, 2000-2018	39
35. Location maps of fire stations in California and Victoria’s study areas	40
36. An interim screenshot of the GitHub repository for this project	45
37. Signup form for Google Earth Engine (as of mid-2019)	46
38. Sample Earth Engine App created as a proof-of-concept	47

Section 1. Introduction

Section 1.1. Key Terms: What is Remote Sensing and Wild-Urban Interface?

Remote sensing has many definitions, of which one of the oldest is from the UN (1986, from their *Treaties Pertaining to the Peaceful Uses of Outer Space*). Approximately:

“The term Remote Sensing means ... making use of properties of electromagnetic waves emitted, reflected or diffracted by ... objects [of the Earth’s surface], for ... improving natural resources management, land use and the protection of the environment.”
(shortened for clarity and emphasis)

Even more modern examples, such as Bettinger’s *Forest Management and Planning* (2017) similarly define remote sensing:

“Remote sensing involves the use of a data collection instrument that does not physically touch the landscape of the feature being “sensed”... [I]nstruments collect reflected electromagnetic energy generated by the sun, or reflected energy that was emitted by a device (such as radar).”

Bettinger continues by noting the two common kinds of satellite-based remote sensing: passive and active. Passive sensors use the light around us, divide it into distinct separate wavelength “bands”, and allocate that data to a unit of minimum ground area (often a “pixel” which represents “a spatial resolution” of n meters) over a repeating time-period “cadence” between renewals of the same area’s image (“temporal resolution”). Active sensors are similar, but instead of taking in the naturally existing light from the sun – they emit signals and wait to see how much (if any) and at what angle the emitted signal returns.

Having noted the above, we may obtain some exciting effects from having images and other such data from remote sensing satellites and their sensors. For example, one of the most popular applications of remote sensing data was proposed by Elvidge (1997): nighttime lights (NTL) can be used to observe where centers of population and commerce are located. Figure 1 shows a nighttime map of six wards near where the University of Tokyo. The imagery and its data were taken in late 2016, using visible light reflectance from a nighttime landcover satellite “Landsat.” The table in Figure 1 was made from the 2015 Census data collected by the Statistics Bureau, Ministry of Internal Affairs and Communications of Japan. Compared to the statistical approach of asking each household to give a count of members, the Remote Sensing approach allows us to see (in general) the relative population density of regions in precise time and spatial scale.

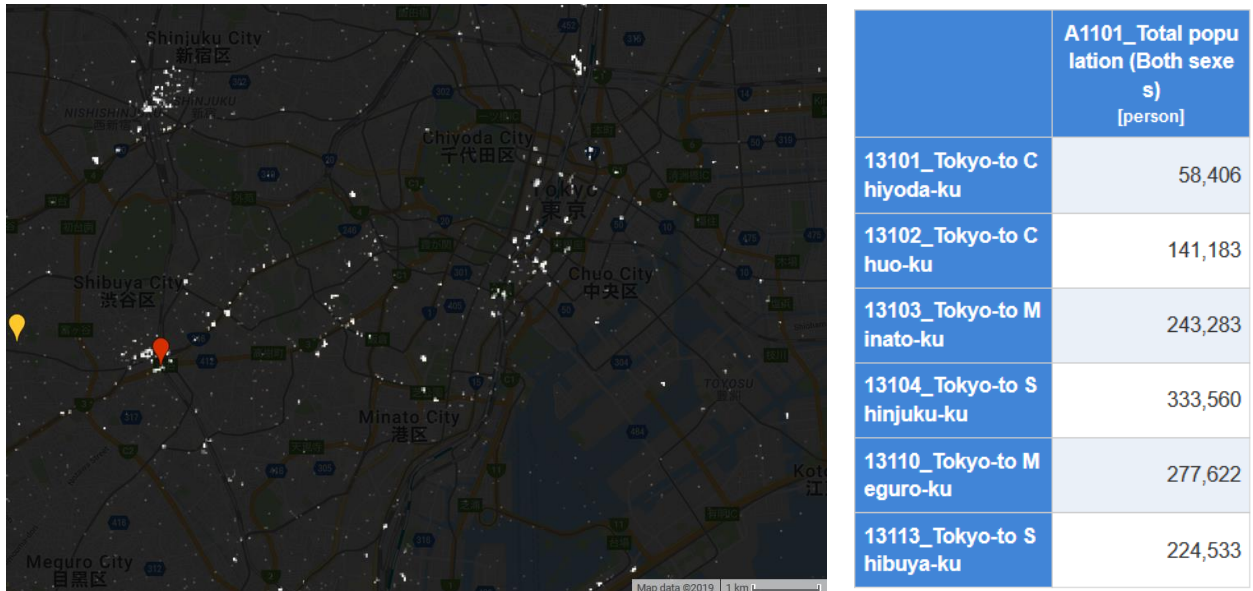


Figure 1. Remote Sensing vs. Classical Data Collection.
 (Left) Remote Sensing shows the relative Population Density on an NTL map. Yellow marker is the University of Tokyo & red marker is the famous Shibuya Crossing.
 (Right) 2015 Statistics Bureau's Census Data for each "ku"-region on the map.

The above image was obtained near-instantly from a computer software package. The creation of tools such as *Google Earth Engine* and *QGIS* have allowed remote sensing professionals greater efficiency to gather information and conduct secondary processing. With an increase in the amounts of available data (both in cadence and in the number of satellites and their sensors), a variety of large-scale, long-term studies have been made possible. When combined with the statistical data collection to provide validation to the research (usually as a percentage of error), this allows us to define new statements about trends and phenomena in our world. This study aims to take full advantage of this development in remote sensing to study a variety of different risk factors.

In comparison to Remote Sensing, the Wild-Urban Interface (WUI) has comparatively fewer definitions, including:

"The wildland-urban interface (WUI) is the area where houses meet or intermingle with undeveloped wildland vegetation..." (Radeloff & US Forest Service, 2005)

A later publication on WUI and wildfires by further detailed that WUI is found:

"...where there are one housing [unit] per 40 acres where wildlands dominate a landscape" (called "intermix") and "[communities on] land with higher housing densities directly adjacent [intermix regions] ... [and the proportion of WUI] is expected to increase further in the years ahead." (Stein and US Forest Service, 2012).

Put another way, WUI is found at the communities which act as a buffer zone between near-uninhabited wildland or forest and nearby relatively populous settlements.

Through the definitions given, we can logically determine that any newly-formed WUI region is the result of either new housing being built in previously uninhabited wildland and forest, or from new growths in vegetation. This question was again answered by Radeloff (2018) when he measured that 97% of new WUI regions are created from newly-built houses. Further, his (2005) previous research mentions that the state of California had the highest number of homes in the WUI, at 5.1 million units and this number remains high (not only in California but across the United States). Worse still, research from Calkin (2014) states that fire occurrence in the WUI is becoming inevitable and troublesome to fight and Schoennagel (2017) says climate change is catalyzing the appearance of yet more fires throughout the WUI. Radeloff further studied the environmental vulnerability factors of climate change and found that not only were temperature and precipitation shift having direct effect on the occurrence of US wildfires in WUI regions, but also that this same climate change was driving populations from larger urban areas into the comparatively temperate WUI regions.

As for the notion of risk itself, one agreed definition from the UN Disaster Relief Organization (1980) mentions that it includes societal exposure, vulnerability, and hazard. Further, Victoria's Colac Otway Shire (2011) refers to hazards as dangerous situations, exposure as a number or percent of people or assets in the region of a hazard, and vulnerability as factors – human, environmental, and otherwise – that makes societies more prone to be damaged when exposed to a hazard. The concept of risk is discussed further in the methodology (see Section 2.3.) of this paper.

Finally, as a surprising finding from Syphard (2009), we have determined that somewhat populated WUI regions were more at risk than the sparsely populated wildlands or the densely populated areas of which they act as a buffer. Syphard suggests that reasons for this risk-imbalance include decreases in the space where embers may travel, urban development removing readily accessible fuel sources for wildfires, and much higher availability of firefighting resources in densely populated regions and the lack of people to notice in the sparsely populated areas. Calkin (2014) notes that beyond this significant challenge, there is also a problem of wildfires spreading over far distances between many communities. This problem is of interest to remote sensing – the in outer-space nature of satellites makes it possible for sensors to efficiently, at low-cost, and periodically monitor multiple communities worth of WUI areas to determine if there would be a risk to any or all these communities. This notion is what forms the basis of this research's desire for modeling risk by predicting future exposure to wildfire – mapping newly-created WUI urban communities' locations in 2030 (the next decade) and 2040 (the decade following).

Section 1.2. Literature Review: Remote Sensing and Vulnerability Analysis of Wildfires, esp. around WUI regions

Arroyo (2008) wrote that most forest fuel mapping had been traditionally performed by on-site fieldwork but had a promising future to be studied by fast-improving sensors onboard remote sensing satellites. He stressed their relative cost-savings, and regular updates while noting that they have limitations in determining specific vegetation characteristics and estimating height. Giglio (2010) wrote that burned area estimate was an essential measure for the hazard for wildfire, leading to his work in creating the MCD45A1 algorithm for processing Moderate Resolution Imaging Spectroradiometer (MODIS) satellite imagery to show where there are burned areas. Giglio (2018) continued his work, and the algorithm for Collection 6 Burned Area was updated to consider active fire locations based on measurements in surface reflectance. Clark (2004) was one of the first to publish on the environmental factors of wildfire, primarily focusing on the influence of wind (spread), temperature (ignition), and soil moisture (fuel) in his predictive models. Levin (2012) then determined factors which controlled wildfire spread –rainfall, land use, and areas with vegetation – all of which may be obtained by GIS maps from satellite products. This was further confirmed by Smith (2014) in his work showing that climate change factors were making vegetation-heavy areas more susceptible to wildfires, commending remote sensing for making it easier to monitor and measure changes in vulnerability over time. He also suggests further research sees a need for predictive modeling of vulnerability factors.

Some of the first work on WUI wildfires was conducted by Myoung (2018) using MODIS vegetation data to measure soil and vegetational moisture content of areas in a WUI near a fire that had occurred in southern California. Similar research in northern California notes that wind-driven wildfires following a delay in autumn precipitation preceded by multi-year drought created fuel moisture conditions caused the WUI in this region to be exceptionally vulnerable (Nauslar, 2018). The existence of private satellites with much higher resolutions than what is commonly available have also been changing this field of study – Michael (2018) notes that with the availability of 10x improved 3m high-resolution satellite imagery they are able to improve the burned area maps and burn severity maps to create a detailed hazard map and estimate of urban forests' exposure to burnt-area. A limitation that previously made scholars dismiss wildfire data in the WUI was the lack of spatial resolution for observing features in the areas of dense wildlands and forests. However, more recent satellites and processing algorithms have improved in this regard. Further, with the help of computational machine learning on remote sensing images, the future of predictive modeling for various factors of wildfire in the WUI looks exciting.

Section 1.3. Objectives and Originality

This study aims to map and identify risk-prone areas in each decade from 2000 to 2040 and to identify new urban expansion in 2030 and 2040 while also considering current hazard and vulnerability factors by accomplishing the following four points:

- (1) Measure hazard time-progression and area affected by fire-progression and classify burn severity for each of the fire-cases that defined these regions.
- (2) Classify the distinct classes of barren/burnt, urbanized, green-covered, and water-covered land cover. Also, show the potential exposure by overlaying the burnt areas from these fires to the simulations of urbanization in 2040.
- (3) Compare environmental vulnerability before and after these fires with changes in temperature, soil moisture, wind direction, and precipitation.
- (4) Calculate a relative density between the location of current (2019) fire stations and the burnt areas from the fires that defined these regions to show if there is any unseen direct social vulnerability.

Further, the originality of this study can be found in the following points:

- (1) The measure of burn-severity (from infrared reflectance), average speed of fire spread, and contemporary (at time of each fire) exposure area for each fire's case.
- (2) Perform cellular-automata artificial neural network (CA-ANN) analysis of urban expansion over a wide spatiotemporal scale using satellite and population data. More specifically, this is studied for 2030 and 2040 using data from 2000 to 2040, for a specific region in California and Victoria near areas burned by each fire.
- (3) Use the results of this urban expansion analysis to identify regions of new expansion (exposure), and regardless of how wildfires may spread in such future areas, consider how the current changes in vulnerability from 2000 to 2020 may affect these and other such surrounding regions if they are to continue in similar manners.

Section 2. Methodology

Section 2.1. Study Area and Timescale

The two selected fires – Black Saturday Fires (in Victoria, 2009) and Camp Fire (in California, 2018) were chosen based on the descending rank order of death toll casualties, measured from the top 20 deadliest fires near wild areas, filtered for only those occurring since 2000 (Ferris et al., 2013 and CAL FIRE, 2018). By comparing more than one location, each on different continents with different climates, it is possible to discover correlations that hold for a wider variety of situations. Attica, Greece was also present in the top 20 – however, as Greece and California share a *Mediterranean climate*, this paper decides to not include Attica in this initial study. Table 1 gives a quick overview of the location, Köppen climate type, and death toll. The positions of nearby urban areas relative these fires were measured via landcover classification but checked against yearly population density maps of Australia and United States from WorldPop project. Similarly, nighttime lighting maps from satellite imagery was used as a proxy to show where variously-sized urban areas are present.

Surprisingly, both fires share a similarity in their effects on WUI communities. In California, the fire started in a forested region just north of the WUI towns of Magalia and Paradise, while threatening the nearby city of Chico (Figure 2). In Victoria, we saw this as multiple fires starting in the WUI communities of Kinglake, Labertouche, Marysville, and other towns while threatening the metropolis of Melbourne (Figure 3). WUI communities suffered the most destruction in both fires, but the nearby populated city region was mostly unaffected. Having satisfied these criteria, both cases were chosen for further research.

Table 1. Location, Climate, and Death Toll of the Top 20 Deadliest Fires on Record (for 2000 - mid-2019)

Fire Name and Year	Location	Köppen Climate Type (Kottek, 2006)	Death Toll
Black Saturday Fires, 2009	Victoria, Australia	Coastal (Cfb)	180
Attica Fires, 2018	Attica, Greece	Mediterranean (Csa)	102
Greek Forest Fires, 2007			84
Camp Fire, 2018	California, United States	Mediterranean (Csa)	85

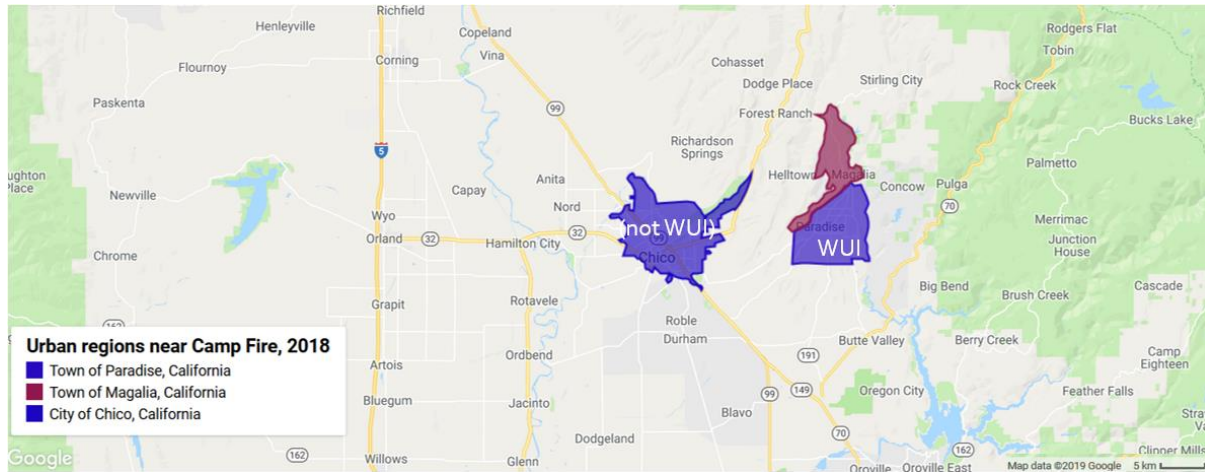


*Figure 2. Regions of Study in Northern California for Camp Fire, 2018.
Note that Magalia and Paradise are WUI due to forest proximity, but Chico is not.*



*Figure 3. Regions of Study in Southern Victoria for Black Saturday Fires, 2009.
Note that many communities are WUI due to forest proximity, but Melbourne is not.*

Within each region, a rectangle was drawn outside the boundaries of all populated areas of interest to each fire, using the online data processing platform *Google Earth Engine*. Figure 4 (next page) visualizes the boundary coordinates for the rectangle drawn around the study area in northern California, while Figure 5 (next page) references the same for southern Victoria. All exports of imagery from satellite products are taken against these borders to keep results for each area uniform and directly comparable.

As mentioned previously, one of the objectives of this paper is to create imagery of the future (which do not yet exist). This required the collection a variety of past data. Table 2 gives a quick review over which years' imagery was collected for each area.

Table 2. Timescale: Years for which Satellite Imagery Collection was Collected in Each Study Region

Year Collected	California, United States	Victoria, Australia
1996	O	X
1998	O	O
2000	O	O
2006	O	X
2008	O	O
2009	X	O, Δ
2010	O	X
2013	O	O
2018	O, Δ	O
2019	O	O

Legend: **X** = not collected; **O** = collected;

Δ = this case study's wildfire year (multiple periods within a year)

When collecting the above imagery, there were multiple images available in each year for almost all satellite products. To better compare each image between different years, the arithmetic mean of all data in the image was computed and the resulting output image was used as the “annual average” image in any given year. Further, for the landcover satellite “Landsat” only imagery that was 5% (Landsat 5/7 imagery, here 1996-2013) or 10% (Landsat 8 imagery, here 2013-2019) clear of clouds were selected for the arithmetic mean function described above. As the Landsat imagery forms a basis for further processing in this study, this “cloud-cleaning” filter was necessary to make sure that information was as accurate as possible – while also not sacrificing seasonal variety nor image availability. The next subsection gives detail on how and from where these images are collected.

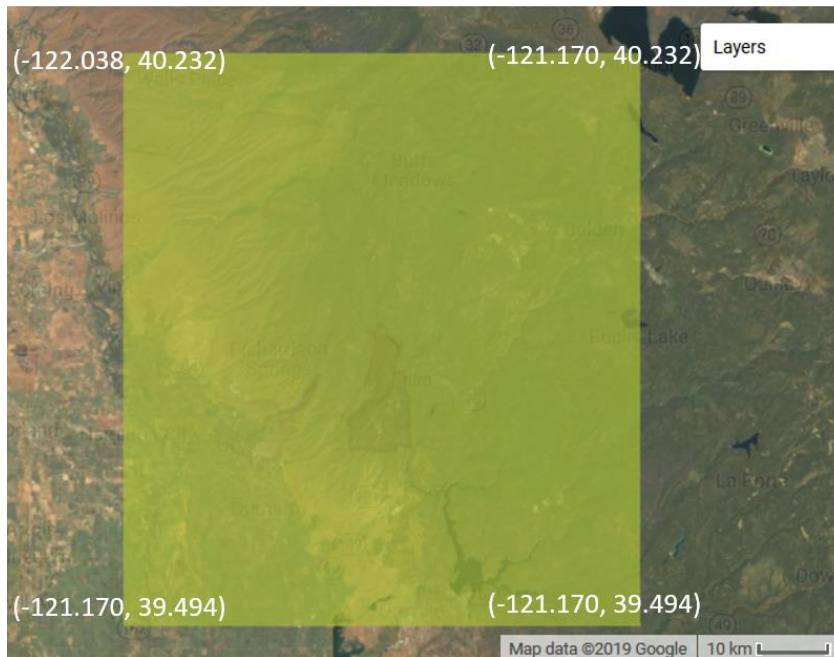


*Figure 4.
The rectangular
boundary for the
Camp Fire's
Region of Interest in
northern California.*

*Background
landcover imagery is
the arithmetic mean
of all Landsat 7
images in (the year)
2000.*

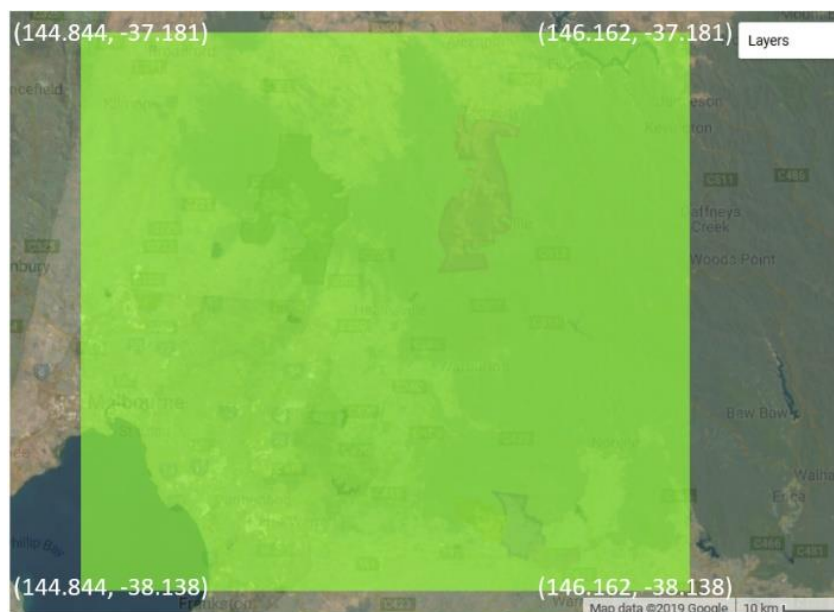


*Figure 5.
The rectangular
boundary for the
Black Saturday Fire's
Region of Interest in
southern Victoria.*

*Background
landcover imagery is
the arithmetic mean
of all Landsat 7
images in (the year)
2000.*

Section 2.2. Sources for Data Collection

Section 2.2.a. Satellite Remote Sensing Data from Google Earth Engine

Most of the hazard and vulnerability analysis was completed with data obtained via Google Earth Engine. Gorelick et al. (2017) created the platform to provide a convenient way to download, filter, run mathematical operations on, and visualize data from remote sensing satellites – which is necessary when there can be as many as 8800 images for some datasets for each region.

The list of this study’s satellite products, cadence and resolution, purpose, and availability period of data is summarized in Table 3. While initial data obtained is as listed in the table, all data was resampled to 30 meters using EPSG:3857-standard “web Mercator” projection. Mercator projection is either elliptical (in 2D) or cylindrical (in 3D) and is unique for placing poles at infinity. Web Mercator is similar but uses a sphere’s coordinates on an ellipsoidal model (Aitchison, 2011).

Table 3. Satellite Products Used, provided through Google Earth Engine

Satellite Product (name)	Cadence (days)	Resolution (m)	Purpose (and availability period)
NASA FIRMS (Fire Information Resource Management System)	1	1000	Daily fire progression in an area [Data available: Nov. 2000 –]
NASA Moderate-resolution Imaging Spectroradiometer (MODIS) Collection 6 Burned-Area	30 31 (1 month)	500	Cumulative area burned by fires [Data available: Nov. 2000 –]
NASA/USGS Landsat Surface Reflectance	16	30	Show Earth’s surface land cover [Data available: July 1972 –]
NASA Global Land Data Assimilation Systems (GLDAS-2.1)	0.125 (3 hours)	~27,500 (.25 arc deg)	Temperature, Soil Moisture [Data available: Jan. 2000 –]
NOAA Real-Time Mesoscale Analysis (RTMA)	~0.04 (1 hour)	2500	Wind Directionality (U.S. only) [Data available: Jun. 2015 –]
JAXA Global Satellite Mapping of Precipitation (GSMaP)	~0.04 (1 hour)	~11,000 (.10 arc deg)	Precipitation [Data available: Mar. 2000 –]

Section 2.2.b. Population Data from WorldPop and VIIRS

While population data is available from multiple sources, a decision to prioritize regular availability, higher resolution, and much simpler visualization of data were made in choosing the WorldPop maps. Stevens et al. and WorldPop (2015) write that with the help of a machine learning method “random forest,” census data for unavailable years (such as those between when a census is formally taken) can be predicted and then mapped at a precise 100m resolution. As described by Stevens, Random Forest is classification tree-diagrams that show factor-based distinct case-scenarios (here, population inflow, migration, and outflow) that can be tuned automatically against various validation data to give each factor dynamic changes in their weights. Also noted, Random Forest is best applied when there are many related predictive factors, each containing a large amount of information. Their work was successfully tested in Vietnam, Cambodia, and Kenya.

The Stevens algorithm was then applied to the rest of the world by WorldPop, a team of researchers from around the world, for each country 2000-2020. Further, WorldPop updates these maps at the close of each year, meaning that these maps are possibly the most up-to-date population maps available for this study. WorldPop can be further compared with the *Gridded Population of the World, version 4* (GPWv4) satellite maps of population and population density. (CIESIN, Columbia University, 2016). GPWv4 (in its most updated revision 11) currently has a resolution of 30 arc-seconds (slightly under 1 kilometer) and a cadence of five years (or 2000, 2005, 2010, 2015, and 2020 (predicted)). WorldPop’s *Global per Country 2000-2020*, however, has a 10x improved resolution of 3 arc-seconds (slightly under 100m) and a cadence of 1 year with annual updates to convert a previously “predicted” year into actual data for each nation.

However, for the supervised training classification, the above data (while very precise) is still too inaccurate for use in secondary processing. As a result, this paper considered Elvidge’s (1997) previous work in proxy population measurement from nighttime lighting and decided it was better to use this measurement as the factor to conduct landcover prediction simulation against. Elvidge specifically recommends the Defense Meteorological Satellite Program - Operational Linescan System (DMSP-OLS) as the satellite sensor of choice to measure the lighting. Additionally, he suggests that even with some significant outliers, it is a dependable choice in a correlative factor for annual measurements of population, GDP, and electrical power consumption in 21 countries across the Americas.

Section 2.2.c. Sample Region Data for Supervised Training Classification

The sample regions of “ground-truth” areas that establish the basis for the supervised-training of landcover into distinct classifications began as Landsat and Copernicus imagery from the Google Earth Pro computer software package. As classification requires comparison of the visible and infrared spectral ranges, there were two separate datasets created for each fire, one for a “normal” case and the other for when the fires had completed their destruction in a “burnt” case. For the “normal” case, the most currently available data and imagery were analyzed for each region, which ended up being across a range of January– October 2018 in California (just before *Camp Fire*) and December 2018 – May 2019 (current imagery) in Victoria. For the “burnt” case, the Google Earth Pro “time slider” feature was used to adjust to the months immediately following the fire. In California, this was a mosaic of December 2018 – May 2019 (after the *Camp Fire*), and in Victoria, this included late February 2009 – early January 2010 (the result of *Black Saturday Fires*).

In each region, the algorithm would search for one of four classifications: barren land (where soil is visible, but also includes “burnt” greenery and the areas of ash where there were previously urban structures); urban area (houses, shopping centers, etc.); green-covered areas (forest, grass, etc.); and water (reservoirs, rivers, lakes, ponds, swimming pools). As Lillesand (2015) suggests, areas used in supervised classification were drawn in complex shapes, but chosen to be large, relatively type-unmixed, and separate from each other. Figure 6 shows an example of each classification type from the *Camp Fire* region’s “normal” dataset (near Paradise, California). Further, the number of polygons created for sample-matching the landcover classification schema are summarized in Table 4.

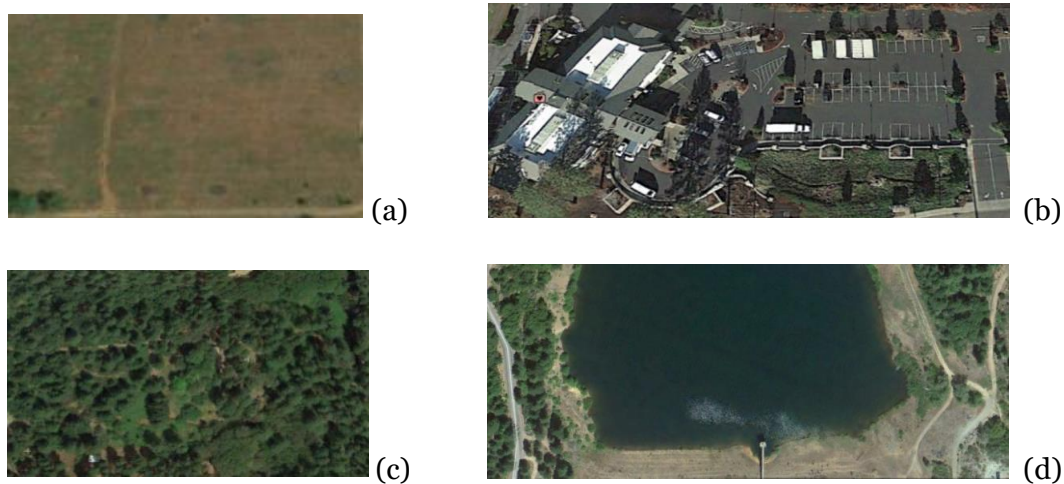


Figure 6. A Sample of Each Classification Type.
[Legend: (a) Barren, (b) Urban, (c) Greenery, and (d) Water]

Table 4. Number of Polygons Drawn as Classification Samples for the “Normal” and “Burnt” Datasets of Case-Study Wildfires

	“Normal” dataset (number of polygons)	“Burnt” dataset (number of polygons)
<i>Camp Fire</i>		
Barren	21	21
Urban	24	18
Greenery	21	20
Water	21	21
Total	87	80
<i>Black Saturday Fires</i>		
Barren	35	35
Urban	25	34
Greenery	27	26
Water	23	20
Total	110	115

Section 2.2.d. Fire Station Location Data from Google Maps

The firefighting staff within fire stations were logically determined by this study to be the initial responders (but certainly not the only) to a major wildfire at the time of its outbreak. As fires are fueled by having an ever-increasing amount of fuel during their spread, rapidly fighting the fire will prevent it from becoming a major disaster for surrounding communities. An assumption is therefore made that if there are many fire stations near or within a WUI community, then it is significantly less vulnerable (compared to a case of their absence). Fire stations were searched in the software program Google Earth, which searches through the Google Maps product online. Often, minor corrections in the location (e.g. “a fire station located at the building adjacent to the software’s marker”) were performed by using street-markings which warn nearby vehicular traffic to “KEEP CLEAR” of the fire truck garage space in front of most fire stations (Figure 7).



*Figure 7.
An example of a
“KEEP CLEAR” sign
at a South Morang,
Victoria fire station.*

Section 2.3. The framework of Analysis: Defining Components of Risk

Continuing with concepts introduced in the Introduction, this section aims to understand how risk as a model of hazard, exposure, and vulnerability may be studied in the context of WUI wildfires.

Section 2.3.a. Hazard Analysis Components

Taking into consideration the previous section, this paper first considers the hazard analysis steps shown in Figure 8.

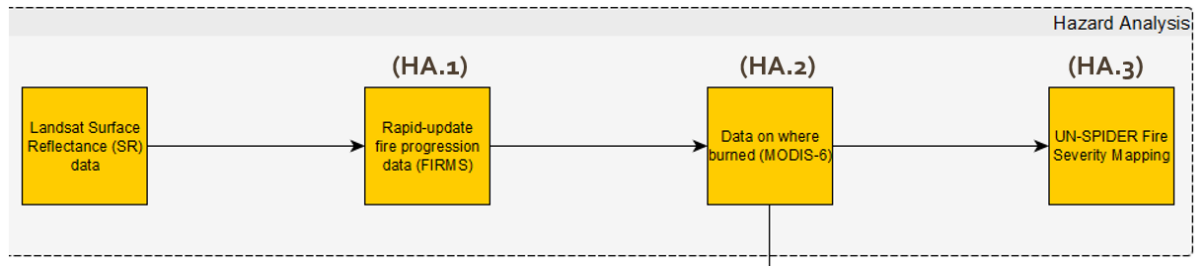


Figure 8. Flowchart of steps used to study Hazard Factors

In starting, this study collected Landsat Surface Reflectance (SR) data to observe the baseline images of the fire (mostly, only the smoke) and to use in further processing at the later steps. Then, in each of the next steps, the following questions were considered:

(HA.1) How long did it take each fire to burn through the towns and cities?

The NASA FIRMS satellite gives the location of where a fire was on each day, but can also show the cumulative areas a fire was in over multiple days. The investigation then measured starting on which day the pixels representing each case-study fire are no longer visible in the area which serves the WUI communities of interest.

(HA.2) How large of an area was burnt?

The monthly MODIS Collection 6 Burned Area product gives us information on where fires had burned for each month. Both fires started after the first of the month, lasted for at least a few weeks (but less than one month), and were significantly greater in magnitude than any individual housefires. Considering that, any burned area reflected from the monthly satellite images present adjacent or within the WUI communities in the region of interest was considered a direct result of the case-study wildfires. Additionally, average wildfire spread speed per day (area burned per day) was calculated with data from (HA.1), above.

(HA.3) How severe was each fire, and how close was each to any major population centers?

The United Nations Space-based Information for Disaster Management and Emergency Response (UN-SPIDER) establishes the burn severity index for measuring the damage to the vegetation in a region after the occurrence of wildfire events. Work by Miller (2007) showed that threshold values of vegetation density change one year before and one year after a fire was a way to measure the damage a fire had to a region. When proposed, it gave rise to a new index called delta Normalized Burn Ration (dNBR), which measures difference per cumulative value between very-near infrared (for Landsat 7, band 4) and mid-infrared (Landsat 7, band 7) instead of Normalized Difference Vegetation Index (NDVI) calculated from the very-near infrared and visible red-bands (for Landsat 7, band 3). The initial proposition of the threshold values of dNBR for each severity level was first proposed slightly earlier, by Key (2005) in his US Forest Service technical report detailing how to make use of the measurement index. A quick look at these dNBR ratio thresholds (Figure 9) show that large negative numbers indicate very successful vegetation regrowth, while large positive numbers show high-impact vegetation mortality.

The distance between major population centers and the WUI communities in the surrounding region of interest was calculated upon this map, with the aid of a measurement tool in Google Earth Pro computer software. This distance was then overlaid as a marker to a straight-line segment between these regions, to visualize severity relative to the proximity.

Severity Level	dNBR Range (scaled by 10^3)	dNBR Range (not scaled)
Enhanced Regrowth, high (post-fire)	-500 to -251	-0.500 to -0.251
Enhanced Regrowth, low (post-fire)	-250 to -101	-0.250 to -0.101
Unburned	-100 to +99	-0.100 to +0.99
Low Severity	+100 to +269	+0.100 to +0.269
Moderate-low Severity	+270 to +439	+0.270 to +0.439
Moderate-high Severity	+440 to +659	+0.440 to +0.659
High Severity	+660 to +1300	+0.660 to +1.300

*Figure 9. dNBR thresholds for each level of burn severity.
The colors for each classification are set by UN-SPIDER, who is the source of this image.*

Section 2.3.b. Exposure Analysis Components

This study then considered exposure factors affecting WUI communities to the risk of wildfire (Figure 10). These were considered through several questions, including:

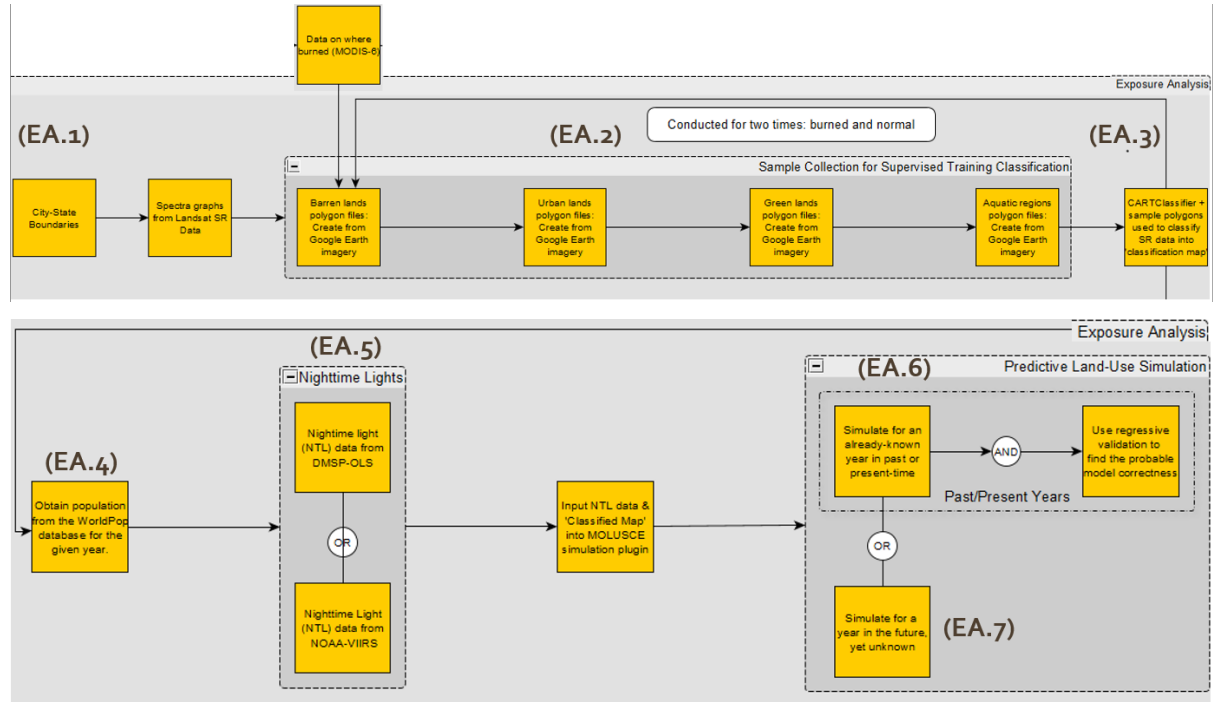


Figure 10. Flowchart of Steps used to study Exposure Factors.

(EA.1) Where are the locations of the towns and cities?

The first step to determining the exposure level for towns and cities is to define where they are using administrative boundaries. Setting a boundary is not easy, because current data is for areas too large: California offers GIS data up to counties (Koordinates, 2018) and Victoria only has the state itself (Government of Australia, 2006). Therefore, all regions' and communities' GIS data were traced using Google Maps data from within Google Earth Pro software program. The resulting polygons were then imported online into Google Earth Engine for further processing with classification methods and other sensors.

(EA.2) How would we decide distinct classes for landcover classification?

This section mostly follows the process first introduced in section 2.2.c. After writing an algorithm which charts and compares the spectra of different land usage features between the communities, we might see that significant difference exists between each type (barren lands, urban housing, greenery, and water) and that barren land has similar spectral signatures to burnt land. Such a comparative spectral chart can be used to justify the decision to classify landcover into the four categories as above.

(EA.3) How can we classify the landcover of these WUI communities?

This section immediately follows the process described in (EA.2). First, the samples taken as validation reference for each class are put into a table with the location of the polygon (a set of coordinates) and a class number that represents a specific type of landcover. For this study, classes were given an arbitrary designation as follows:

0 (zero) = barren (or burnt, if applicable)

1 (one) = urban region

2 (two) = greenery region (e.g. grass or forest)

3 (three) = water-covered region

This information was then fed into a native algorithm built into Google Earth Engine, “CARTClassification,” or Classification and Regression Tree method. This method pioneered by Breiman et al. (1984) not only considers the creation and categorization of factors into a decision tree but also states that the target variables are continuous and hence regression between factors in the tree can be used to help predict the value. In other words, the sample points defined previously are set at exactly each arbitrary whole number; but all the unknown areas are plotted at values between these numbers. Whichever whole integer number value these unknown points lie closest to is the class we receive as a result from running the algorithm.

(EA.4) How has the number of people living in these WUI communities changed over the years?

Exposure is not only the area of the places where the people lived but also how many people will be affected as well. The WorldPop database (also see section 2.2.b.) provides a graphical measurement of this value, showing a relative population density as a brighter signal where higher. We first download entire-country maps from the WorldPop webpage for each of (years) 2000, 20008, 2009, 2010, 2018, and 2019 (the union of the sets for the *Camp Fire* and *Black Saturday Fire* from Table 2 in section 2.1.). The regions of interest were cropped, and these images were ingested into Google Earth Engine as data-tagged “assets”. The assets’ density data is then used to confirm the existence of people in the various WUI communities identified earlier (see section 1.3.) and to verify that their relative density is more than that of the adjacent wildland but less than that of the neighboring city or metropolis they border.

(EA.5) How does visible nighttime light change over the years in these WUI communities?

Nighttime lights (NTL), as previously discussed, are an established measurement tool for population density. The availability is slightly longer than the WorldPop database, as it extends into a few years before 2000 (starting in 1992) and their resolution of 30 arc seconds (~ 100 meters) is enough to see detail in population density even within each WUI community. This study obtained DMSP-OLS imagery (1996-2013) or Visible Infrared Imaging Radiometer Suite (VIIRS) imagery (2013-present) for the years detailed in table 5, averaged the monthly data into one annual image, and used the result measures of density as a factor for further analysis in the next step – the creation of a predictive classification for future years with aid from a CA-ANN machine learning program.

Table 5. In Which Years DMSP-OLS and VIIRS Images were Downloaded for each Case-Study Wildfire

	<i>Camp Fire, California</i>	<i>Black Saturday Fires, Victoria</i>
<i>Year</i>		
1996	D	
1998	D	D
2000	D	D
2006	D	
2008	D	D
2009		D
2013	D, V	D, V
2018	V	V
2019	V	V

Legend: **D** = DMSP-OLS imagery collected; **V** = VIIRS imagery collected;

[Blank] = no imagery collected

(EA.6) Why and how can we model change using neural network machine learning programs upon a given set of landcover images?

Landcover shows us the urban regions which would be exposed to a natural disaster, were one to occur in a region of interest, such as the WUI communities of this study. With modern programming and image processing techniques such as the Cellular-Automata Artificial Neural Network (CA-ANN) machine learning programs, Myint et al. (2006) suggests that we can use two previous landcover images separated by a period of n years (for n an arbitrary non-zero, positive integer) and correlating (but not same) factor image[s] from the earlier year to determine what the landcover for a region of interest would look like n years after the more recent image. Knowing this likely will elucidate novel areas prone to future urban creation or expansion. CA-ANN algorithms come in a variety of forms and uses, but their general purpose is to abstract any input data into a flattened collection of one-dimensional features based on a correlative factor, then to transform the original data by repetitive matrix operations relative the magnitude of the factors' correlation (depicted in Figure 11). Here, this project uses the Modules for Land Use Change Simulations (MOLUSCE, 2013) python CA-ANN algorithms made by NextGIS and Asia Air Survey. Running MOLUSCE in a compatible version of QGIS software package (this paper used version 2.18.27), we input landcover and DMSP-OLS NTL-based population images of a 10-year and 5-year validation scale for each of the case-study regions and set parameters to have the program conduct 50,000 generations (matrix operations). These simulated images were then compared with “real” images (from 2018, the most recent complete year) to measure percentage accuracy in each area. Put another way, the MOLUSCE algorithm was ran in both case-study regions for [a] 1998 and 2008 (10-year scale) and [b] 2008-2013 (5-year scale) and [c] the 2018 “real” (both Landsat 7 and Landsat 8) images and “simulated” image were compared for matched-pixels (the *percentage of accuracy*) to test the validation.

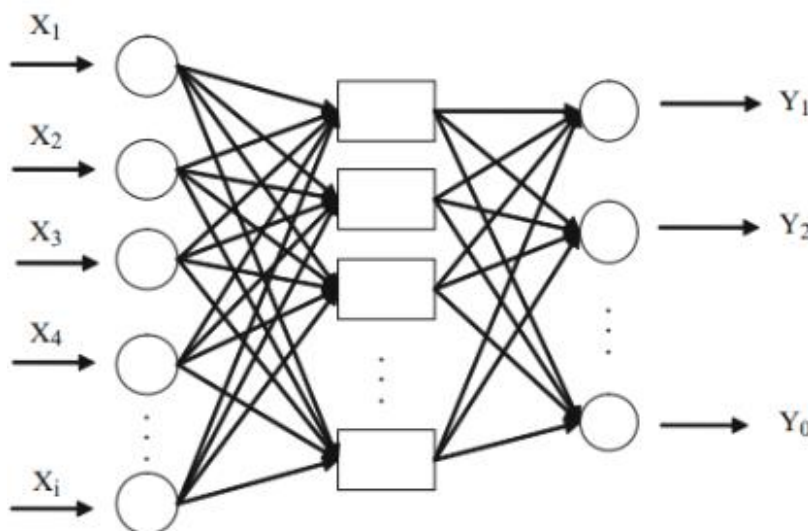


Figure 11.
Generalized
depiction of a model
Artificial Neural
Network (ANN).
Shows the input data
and factors,
abstracting matrix
operations, and
output weights.

(EA.7) How can we use neural network machine learning programs upon a given set of landcover images to further model future years' change?

Considering the above, we now understand that work by Myint et al. and NextGIS show the value and feasibility of using CA-ANN machine learning programs to determine “*n*-years later” exposure. It is a trivial application to use more disparate years of landcover imagery to obtain landcover images for years beyond the current date. Once again, the MOLUSCE program was employed to run a CA-ANN with 50,000 generations to model 2030 and 2040. In Victoria, 2030 was modeled with 2008 and 2019 and 2040 with 1998 and 2019, while in California, 2030 was modeled with 2006 and 2018 (January-October) and 2040 with 1996 and 2018 (January-October). The shift was necessary for California to prevent the dramatic effect the November 2018 *Camp Fire* had on the landcover (especially vegetation) within the simulation.

Section 2.3.c. Vulnerability Analysis Components

Lastly, this study considers the vulnerability factors of WUI communities to the risk of wildfire (Figure 12). These were also examined through several questions, including:

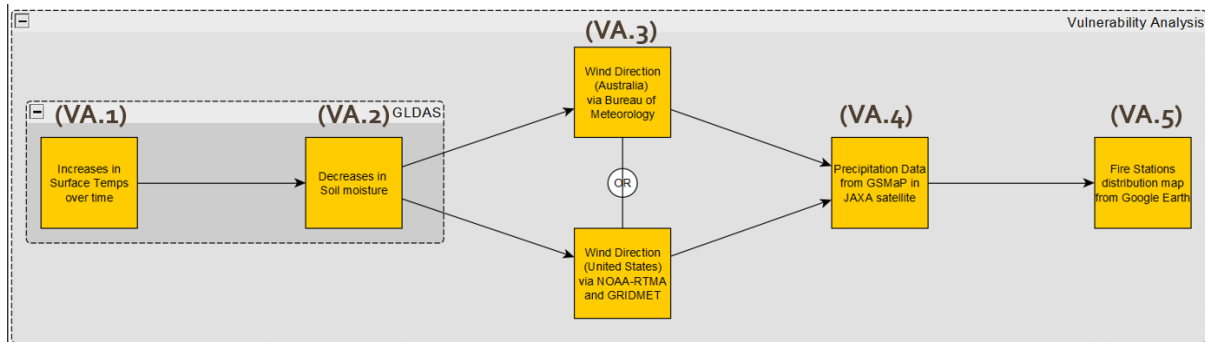


Figure 12. Flowchart of Steps used to study Vulnerability Factors.

(VA.1) Where do we see increases in the at-surface temperature?

Amongst environmental vulnerability factors, the temperature plays a significant role in making an area more vulnerable for a fire to occur or spread by acting as the heat needed to catalyze biomass combustion. The NASA GLDAS-2.1 satellite sensor has been collecting various temperature, soil moisture, snow depth, runoff, pressure, humidity, and other different indices of environmental systems. Google Earth Engine helped assimilate the cumulative data over any given year (which at 3-hour cadence was a little over 2500 images) and then make an annual average map for 2000, 2009 (Victoria), 2010 (California only), and 2018. Finally, comparative observations were made between the images to determine any possible short- and long-term trends.

(VA.2) Where do we see decreases in the at-surface soil moisture?

As fires traverse across the landscape, dry biomass will help fuel a quick spread. Decreases in soil moisture would place a region at higher vulnerability for uncontrollable wildfires and their damage. The NASA GLDAS-2.1 satellite sensor also measures soil moisture, and this paper again used Google Earth Engine algorithms to assimilate cumulative data (of over 2500 images) into a single annual average map for each of the same periods as the at-surface temperature (section 2.3.c (VA.1), previous page). As before, comparative observations were made for these images.

(VA.3) How does the direction of the wind affect WUI wildfires?

Previous simulations of wildfire show that the direction the wind will blow in has effects on the spread (or temporary halt) of fire (Clark et al., 2014). The NOAA's RTMA satellite sensor has started to measure the direction of wind over the continental United States every hour since mid-2015. This satellite can give frequently updated data of how the wind changed during the *Camp Fire*, though to simplify the model of this vulnerability only the average wind direction for the first day of wildfire occurrence was considered. However, even in the present day, there is no satellite which measures wind direction outside the United States (let alone in 2009) – so the *Black Saturday Fires* didn't have satellite data available. However, the Australian Bureau of Meteorology released a wind direction map of its first day, allowing a comparison to be drawn between the fires. The results are placed alongside the matching FIRMS fire progression image (see section 2.3.a (HA.1).) to draw comparative conclusions about wind direction to the directions fire progressed in.

(VA.4) How does the amount of precipitation affect the spread of wildfire?

Considering that fires have a significantly harder time to access the oxygen in biomass fuel when said fuel is damp, we might assume that a larger amount of precipitation would prevent the occurrence, stunt spread, and put out the fires quicker. However, this correlation needs verification before a lack of rainfall can be called a vulnerability factor of fires. The JAXA GSMaP satellite sensor series has been measuring global rainfall rate in millimeters per hour since early 2000, with a measurement every hour. Using Google Earth Engine to average all almost 9000 annual cumulative images into a single yearly image, and the number of hours in the time being studied (whether 8766 hours in a year or 730 hours in a month) were multiplied to the average rates to obtain the average cumulative rainfall value. Data is then compared for the periods detailed in the above sections on soil moisture and temperature (this section, (VA.1) and (VA.2)) for comparative observations of any short- or long-term trends.

(VA.5) How does the density of fire stations in a region closest to the WUI communities affect their vulnerability to wildfire?

Considering that wildfires spread quickly once initially sparked, more firefighting professionals available to quickly arrive on-the-scene means less damage the fire will ever cause to the surrounding communities. This is especially important in WUI communities, whose locations are separated from larger populations and can occasionally even lack their firefighting resources. Notwithstanding the existence of many other city planning indicators that can show vulnerability – this first-mover effect from being the earliest part of a human-powered chain of actions that happen in a large-scale disaster (in the WUI and otherwise) makes fire station density a relatively important measurement of the social-human nature of vulnerability. For both case-studies, fire station locations were searched in Google Maps for the entire region of interest, placed in a table that represented the fire stations locations with a set of coordinates in complex polygonal shapes, and uploaded into the mapping system present in the online Google Earth Engine platform. From here, two factors were calculated – a density of how much area each fire station would have to serve and how much area each fire station can serve, if they are to arrive on-scene within standard response times. A second calculation of density was also taken from the ratio of the study area to the number of fire stations situated within the WUI.

Section 3. Results and Discussion

Following the previous sections, this section aims to provide the results after applying the methodology for each of the case-study regions. Most images shown in the section are cropped from the original study area (detailed in section 2.1.) to show greater detail and improve visibility. Short comments giving further detail and analysis are provided for each sub-section, based on discoveries made during the process of obtaining the results.

Section 3.1. Wildfire Spread, Area Burnt, and Burn Severity | (HA.1) – (HA.3)

Figure 13 shows the NASA FIRMS sensed imagery for the progression of the Camp Fire around the communities of interest. The (a) first and (b) second day see fast and widespread growth to the fire over these communities, while on (c) days 3 to 10 [cumulative] we see successful firefighting efforts have scaled back the fire to a northern (almost uninhabited) region of the community. By (d) days 11 to 15 [cumulative, at end of the fire], we see that firefighting efforts in WUI communities have succeeded: remnants of the fire burn tamely in the surrounding forests. The other thing that FIRMS imagery will show is the brightness intensity of the flames, which is correlated (but not the same as) the temperature of the fire on the ground. The red “warm” refers to brightness values of 300-370 Kelvin (K), the orange “hot” refers to amounts of 370-440 K, and the white “very hot” refers to 440-510K. Figure 14 shows similar results for the *Black Saturday Fires* in Victoria.

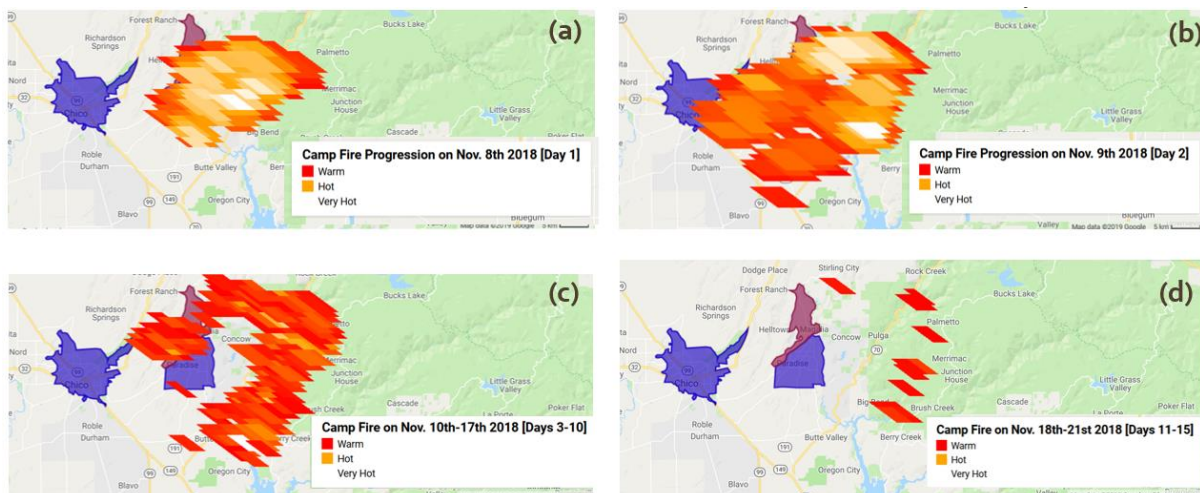


Figure 13. Camp Fire wildfire spread, esp. near WUI communities.

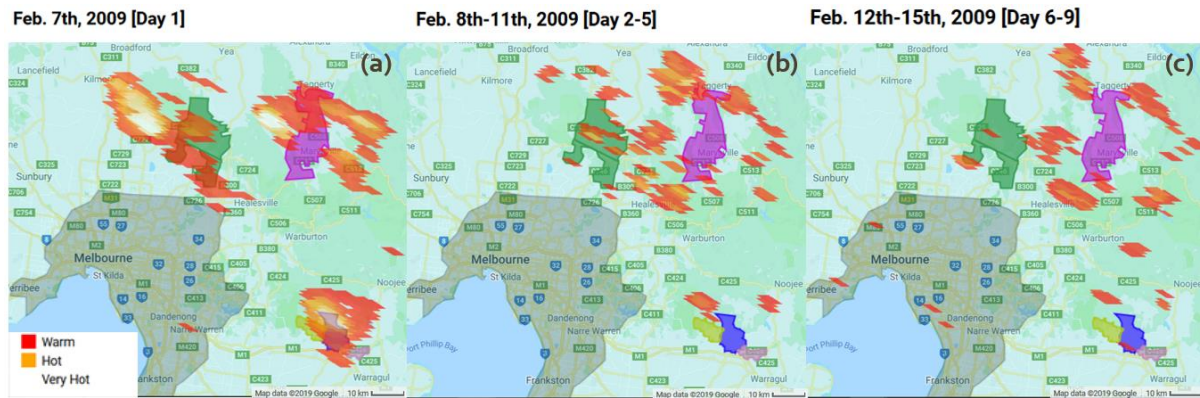


Figure 14. Black Saturday Fires wildfire spread, esp. near WUI communities.

In Figure 14, on (a) the first day we see a quick explosion of fire, especially in the Labertouche communities (each image's bottom-right) and across the western Kinglake (top-left) and northern Marysville (top-right) communities. The brightness values representing “warm,” “hot,” and “very hot” remain the same as before - showing that the burst in fire’s heat was an intense, but short-lived only throughout the first day. The (b) cumulative days 2 to 5 image shows firefighting efforts are already succeeding on the second day in Labertouche and are assisting in limiting the spread and lowering the temperature of the flames in the northern WUI communities. By (c) cumulative period days 6 to 9, we see that the firefighting efforts have moved the fire out of the WUI communities and into the forests, where sporadic firefights would continue until the end of the 5th week. We see the Camp Fire progress rapidly through the WUI communities it affected, burning in them the first two days and then being eradicated within those communities on the third. Meanwhile, the Black Saturday Fires flared up equally hot on their first day but were already beginning to recede with firefighting efforts on the second day - continuing until the end of the first week.

The area burnt by these fires was measured by the Burned Area algorithm that NASA runs on the monthly-average (arithmetic mean) of its MODIS satellite sensors’ data. After receiving the monthly image output for each case-study fire had burned, the image was exported as an image file for further processing in the Google Earth Pro software package. This research used the “ruler” measurement tool to draw a polygonal shape around the outside of each distinct blackened area, which represents the continuous burnt area – from which the “ruler” outputs a value representing such a polygon’s area. Values were rounded to the nearest 5 square kilometers. As Figure 15 shows, the total burned area within California’s study region was near 515 square kilometers, and as Figure 16 shows, the total burned area within the Victoria study area was about 1975 square kilometers. This means that the *Camp Fire* averaged 206 sq. km. per day and *Black Saturday Fires* averaged 282 sq. km. per day.

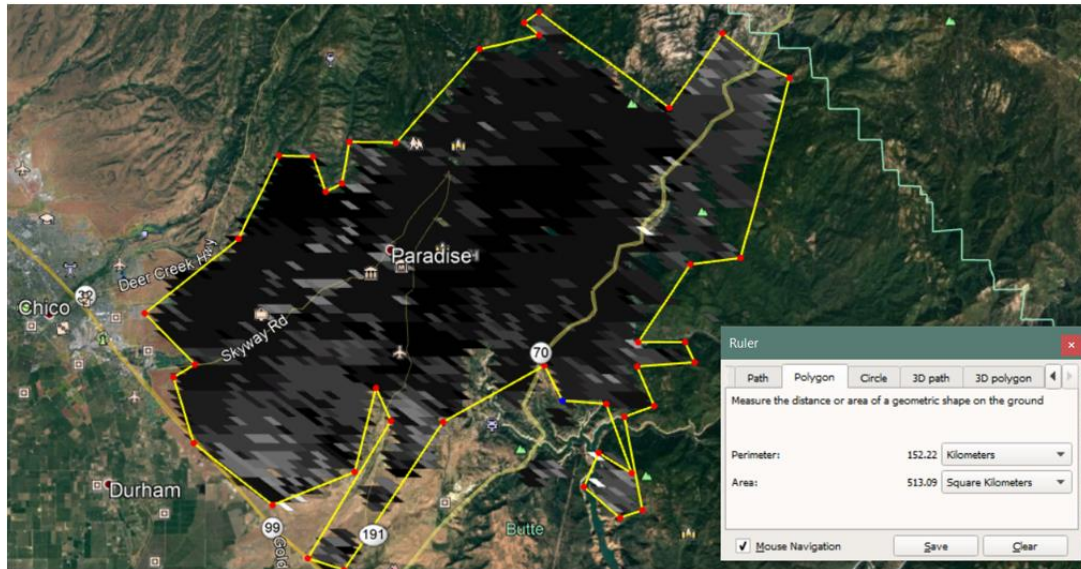


Figure 15. Camp Fire burned area polygon measured with ruler in Google Earth.

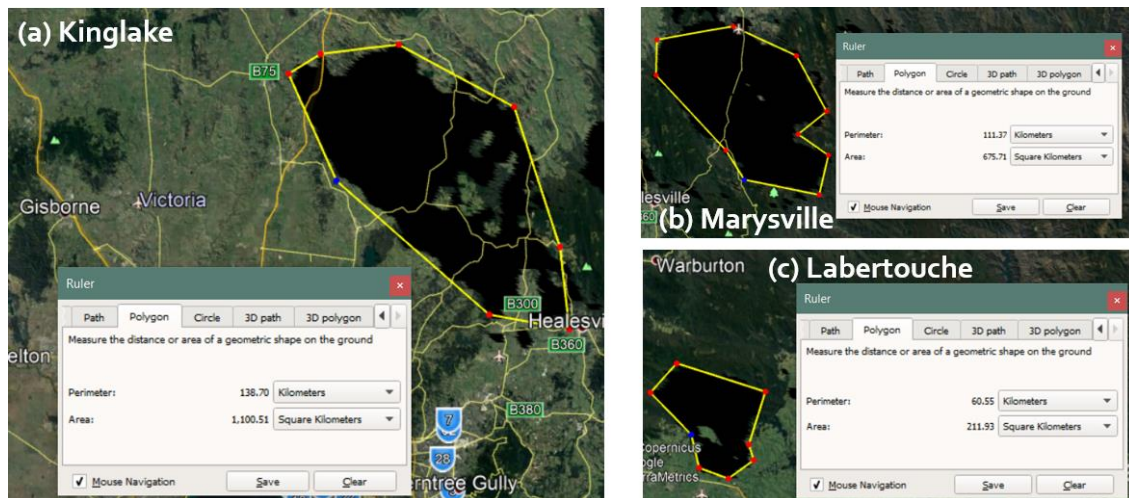


Figure 16. Black Saturday Fires burned area polygon measured with ruler in Google Earth.

The burn severity (Figure 17) in both fire-cases was severe. Both Paradise, California and a surrounding uninhabited region near Paradise Airport, and in every WUI community of interest in Victoria (Kinglake, Marysville, and Labertouche areas) there was high severity impact according to the difference of the infrared values measured in vegetation before and after the fires. While some wildfire is a natural ecological process, sustained and repetitive high-severity fires could potentially change the landscape to a permanently barren area. Further, nearly 100,000 people live in the college town of Chico (Yale, 2018) only 20km away (measured with “ruler”) and around 5 million people live in the Victorian state capital of Melbourne (Population Australia, 2018) some 55-100km away. Protecting the WUI areas is a first step to assure the safety of those living in these much more populated centers.

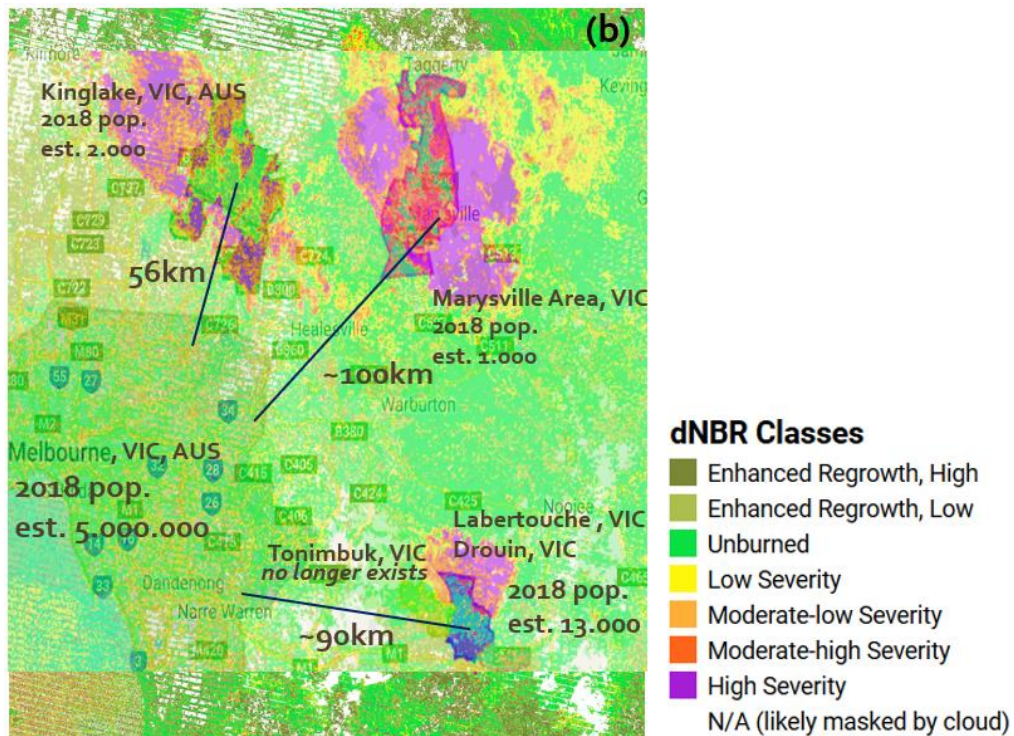
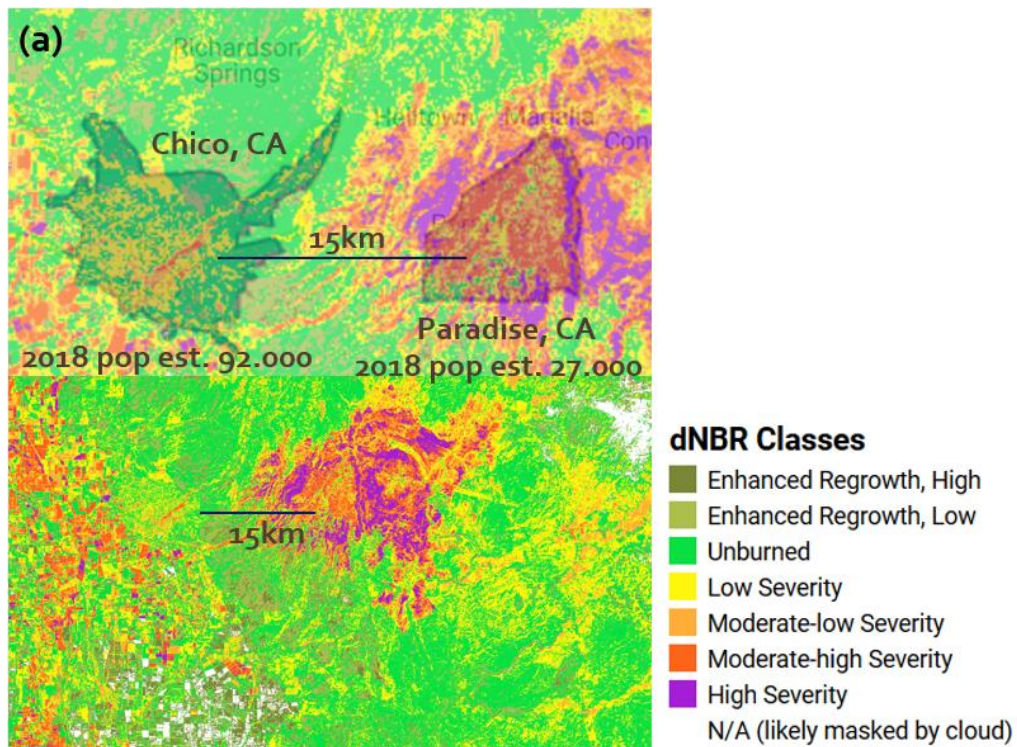


Figure 17. Burn severity and locations of surrounding area maps.
The top is from Camp Fire; Bottom is from Black Saturday Fires.
All population and distance data were collected for 2018.

Section 3.2. Spectra and Overall Review of Landcover Classification Result | (EA.2) – (EA.3)

As previously described (section 2.3.b (EA.2)), spectra graphs such as the one shown in Figure 18 can give us an idea of if our classes used in supervised classification have significantly different properties. The Landsat satellites (here Landsat 8) collect Surface Reflectance data on a scale of 0 to 10,000. However, if reflectance is a ratio between 0 and 1, a linear re-scaling is necessary to obtain percentages. We see that in the pre-Fire spectra, the visible regions have a small but significant difference in reflectance (a few percentage points) between each other and the infrared regions have a much more pronounced level of variation (up to nearly 25 percentage points between lowest and highest).

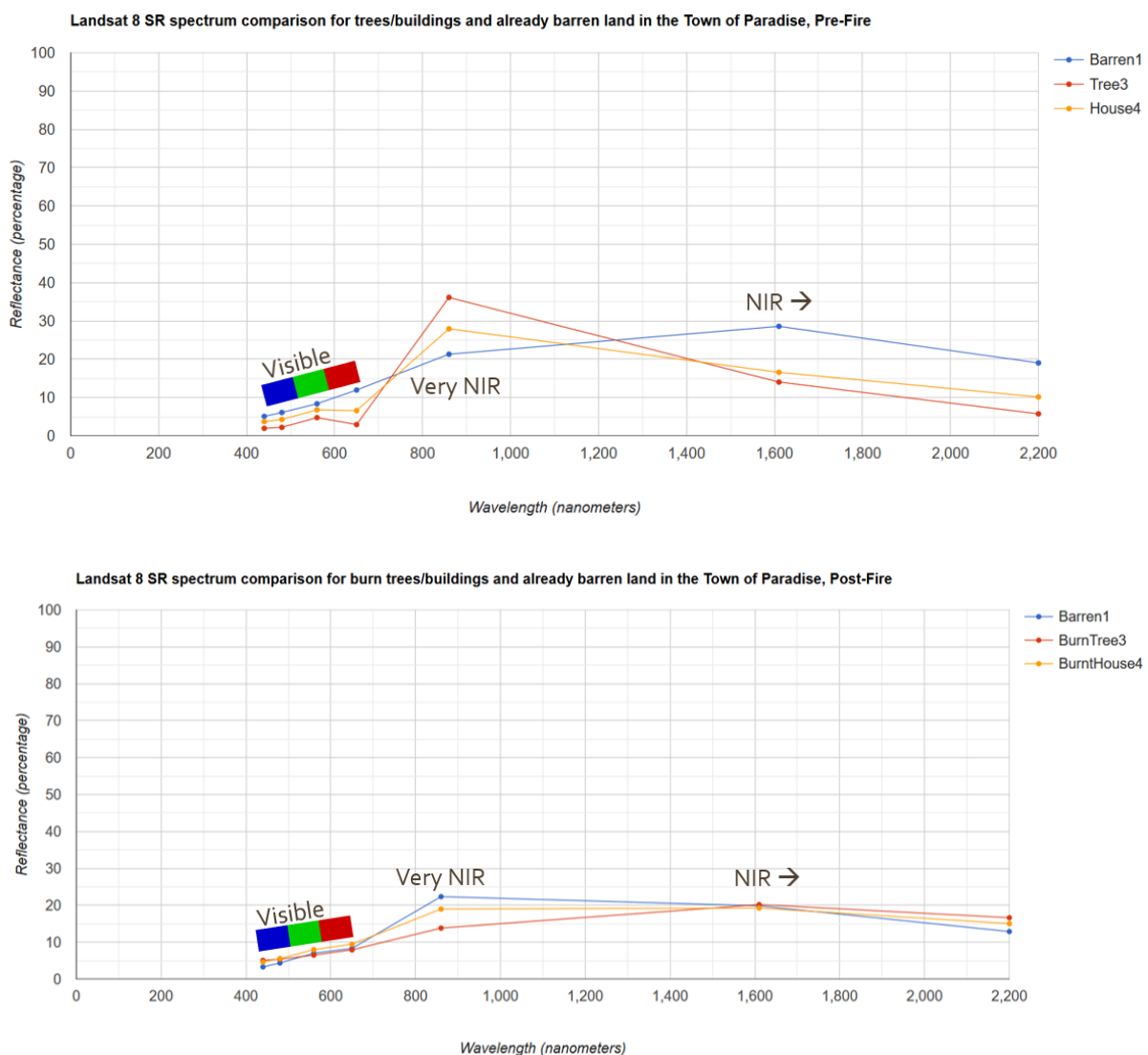


Figure 18. Spectra graphs of Landsat 8 Surface Reflectance (SR) in Paradise, California. Top chart uses satellite imagery from before Camp Fire; the bottom graph was from after. Both graphs show curves for the same sample barren field, tree, and house.

While we see that the range of reflectance values are significantly dampened in the post-fire burnt surface reflectance imagery, we see that the very near-infrared (vNIR) and 2200 nanometer (nm) medium-infrared had pronounced differences of up to 10 percentage points range and a few percentage points ranges, respectively. This is because burnt ground (barren as it may be), trees, and houses all have a similar black charcoal color to the visible light spectrum (what the human eye sees) but their materials have different heat-reflectance properties (soil, plant and other biomass (even dead plants), and artificially-created construction materials such as concrete). Considering the previous, it was decided that the supervised classification can accurately and should search for barren (or similarly reflective burnt) regions, (artificially-constructed and mostly populated) urban regions, (forests, grass, and other biomass-like) greenery regions, and (lakes, reservoirs, pools, and rivers-like) aquatic regions. These were fed into the CART (Classification and Regression Tree)-type classifier to convert various Landsat 5, 7, and 8 images (depending on the year) into colorful images that showed types of surface reflectance classification. (See table 6 for a summary of what colors this paper assigned to each classification-type.)

Table 6. Color Assigned to Each Landcover Classification (with Sample)

	Color	Sample
<i>Classification</i>		
Barren	Brown	
Urban	Yellow	
Greenery	Green	
Aquatic	Light Blue	

Figure 19 shows a series of the landcover classification images for California in 2000, 2010, 2018 (pre-fire), and 2018 (post-fire). Figure 20 shows a similar set of images for Victoria in 2000, 2008 (pre-fire), 2009 (post-fire), and 2018. Perhaps the most apparent difference is the after-effect of the fires made in 2018 (in California) and 2009 (in Victoria), where we see large burn scars that have converted vast swaths of greenery into barren land. However, both areas also show populated cities are expanding, smaller WUI communities are often newly established in the last 20 years, and even without fires, there was a trend for greenery to die and become barren land areas. For example, Paradise (California, dark shaded area in the image) wasn't that big even in 2010, yet the pre-fire image of 2018 had shown a significant cluster of urban settlements in the southern part of the city.

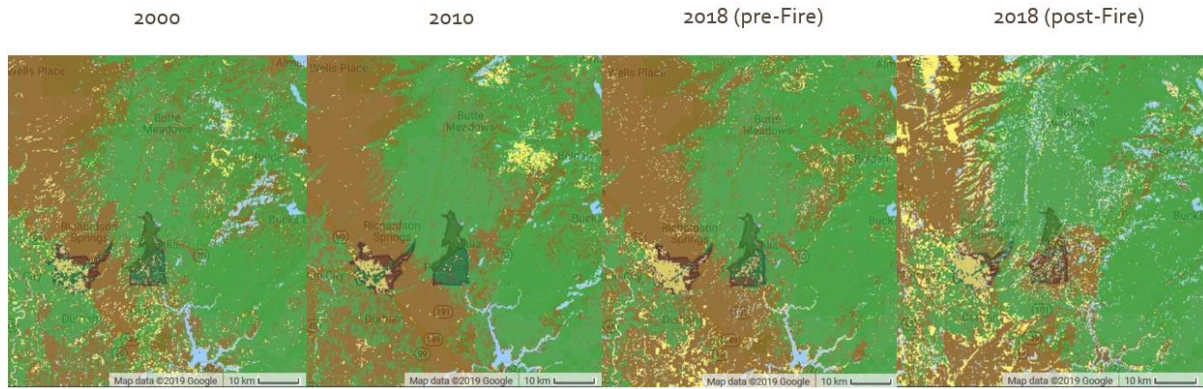


Figure 19. Landcover change in Camp Fire study area from 2000 – 2018.

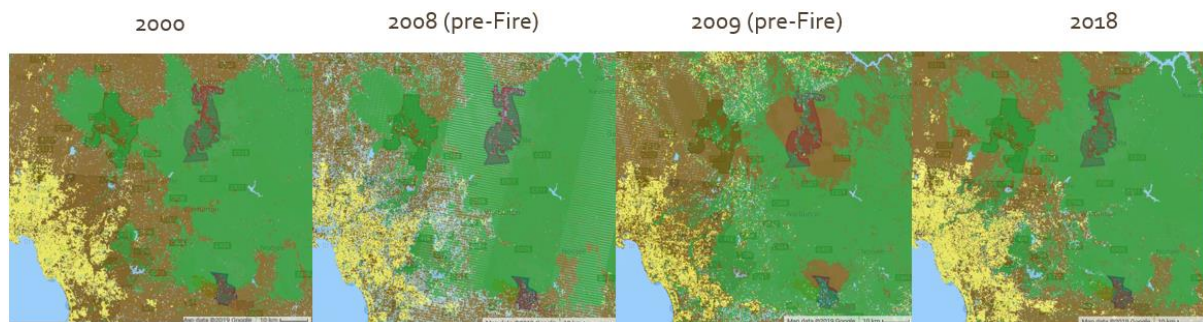


Figure 20. Landcover change in Black Saturday Fires study area from 2000 – 2018.

Section 3.3. Population Exposed within each WUI Wildfire Study Area | (EA.4) – (EA.5)

By understanding changes in the population, this study aims to understand the level of exposure at the time of each fire, and indeed, to observe if Radeloff's observations hold – if there have been WUI communities expanding/created since the start of this millennium.

Figure 21 shows California's WorldPop images of population count per pixel (a relative measure of population density) for 2000, 2010, and 2018 (pre-fire).

The latest update was in very early November 2018, so the post-fire effect has not yet been reflected. Figure 22 shows the WorldPop images for Victoria in those same years.

The WorldPop database seems to show very similar images for all areas, indicating a relatively dense WUI region in the Paradise, California area and surprisingly very little population density in most parts of the Victoria study area. Considering these potential inaccuracies and the lack of data post-fire for California (due to availability being limited to the year before the fire), this thesis decides to instead consider nighttime lights as a proxy for population density in these areas.



Figure 21. WorldPop population density of Camp Fire study area.



Figure 22. WorldPop population density of Black Saturday Fires study area.

Two satellite sensor products are available to measure proxy lighting since 2000: DMSP-OLS measured visible and near-infrared until 2013 and VIIRS Night Band measured from 2013 onwards. Figure 23 shows proxy lighting in the California study area 2000, 2008, 2018 (pre-fire), and 2018 (post-fire). Figure 24 shows similar measurements in 2000, 2008 (pre-fire), 2009 (post-fire), and 2018. We can see the change in resolution between the DMSP-OLS sensed images and the VIIRS sensed images by comparing the sharpness of the lighting. Hence, the WUI community of Paradise looks to have shrunk from a diffused population into a concentrated population in the south – however, this is likely not the case. We also see the small growth, destruction, and a restoration of the WUI communities in Victoria for the periods before the fire, right after the fire, and currently. While the population density is not heavy, such as within Chico or Melbourne, the WUI communities show increasing inhabitation throughout the previous decades.

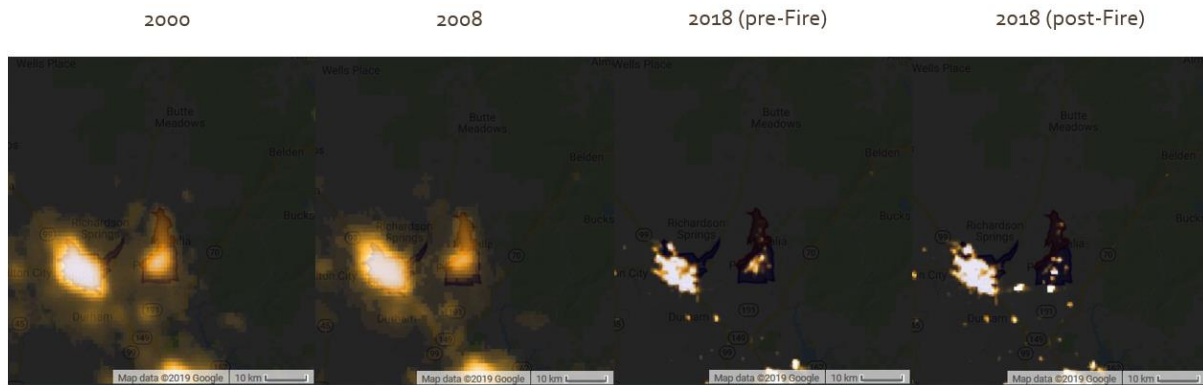


Figure 23. Proxy Population by NTL Change in Camp Fire study area.

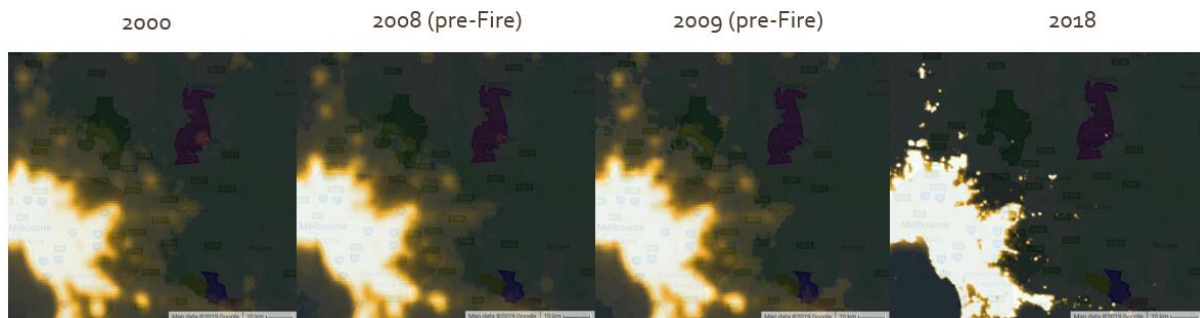


Figure 24. Proxy Population by NTL Change in Camp Fire study area.

Section 3.4. Predictive Changes in Urban-Area in the Wild-Urban Interfaces | (EA.6) – (EA.7)

Using a CA-ANN program, simulations were run for California and Victoria in 2018, 2030, and 2040. The 2018 images were run to test the algorithm because the simulated images could be validated against the “real” images sensed by the Landsat satellites in 2018 (both Landsat 7 and 8). Table 7 shows the validation results as a percentage of accuracy measure, for “simulated” image vs. the “real” images in both regions. We note that the satellite image used affected the accuracy percentages by a few points. While 2008-2013 imagery is more accurate (perhaps due to the smaller amount of time to be predicted with the same number of generational simulation cycles), California had a more accurate simulation when compared to Landsat 7 imagery (at 79.06%) and Victoria was more accurate when compared to Landsat 8 (at 80.26%).

Further, as we can see from the comparison of “simulated” vs. “real” images in California (Figure 25) and Victoria (Figure 26), the simulation often overexpressed the urban signal, with expression in random areas. Hence, areas of potential novel urban development were limited to regions with 0.15 sq. km. or more of a concentrated urban signal.

Figure 27 shows the landcover predictions for 2030, and Figure 28 shows the predictions in 2040, with each image displaying California on the left and Victoria on the right. Further, Figures 29 (in California) and 30 (in Victoria) show areas with potential for new urban expansion or creation. This included densification and expansion around all sides of Chico (blue square), potential expansion (assuming rebuilding) in Paradise (the orange square in the middle-right), and perhaps some novel WUI creation in the Oroville area (the middle-lower orange square). However, the Oroville area is not in the currently known area of exposure from the *Camp Fire*, so it is not as risky as potential WUI rebuilding in Paradise. In Victoria, we see Melbourne expand (primarily to the north (upper-right orange square) and northeast (upper-right blue square)), though only the northeast nears the zone of exposure around the Kinglake area; Marysville (in the zone of exposure) likely becomes denser (but does not expand, shown in the upper-right left square), the Labertouche area (also in zone of exposure) densifies and extends horizontally (the bottom two orange squares and one blue square), and a novel area of WUI urbanization is shown adjacent to the southern boundary of the Kinglake zone of exposure (central orange square). As currently available data would suggest, these are the regions which should be aware that they are at higher risk to wildfires, due to their exposure based on the previous case-study history of where each fire had burned. However, exposure does not guarantee vulnerability since the environment (or humans) can mitigate (or give higher susceptibility to) risk.

**Table 7. Satellite-Dependent Landcover Simulation’s Validation
(in Percentage of Accuracy), for each Case-Study WUI Region**

“real” images -->	Landsat 7 (%)	Landsat 8 (%)
<i>Region</i>		
Camp Fire (California)		
1998-2008	78.13892	76.78931
2008-2013	79.06125	78.84803
Black Saturday Fires (Victoria)		
1998-2008	67.81663	72.00730
2008-2013	76.26121	80.26044

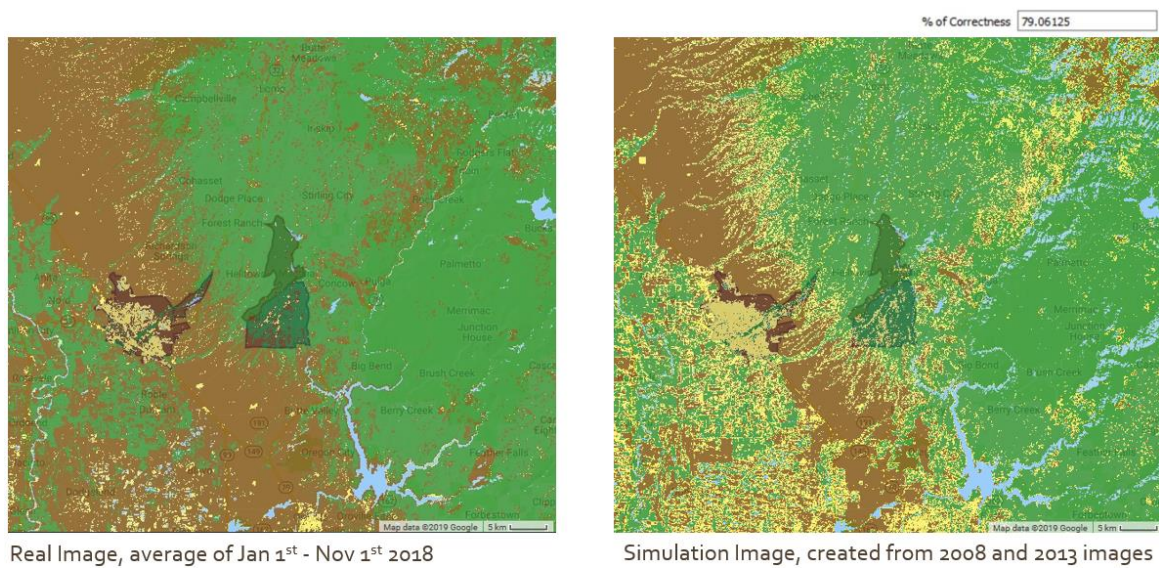


Figure 25. “Real” vs. “Simulated” image in California, comparing classification accuracy.

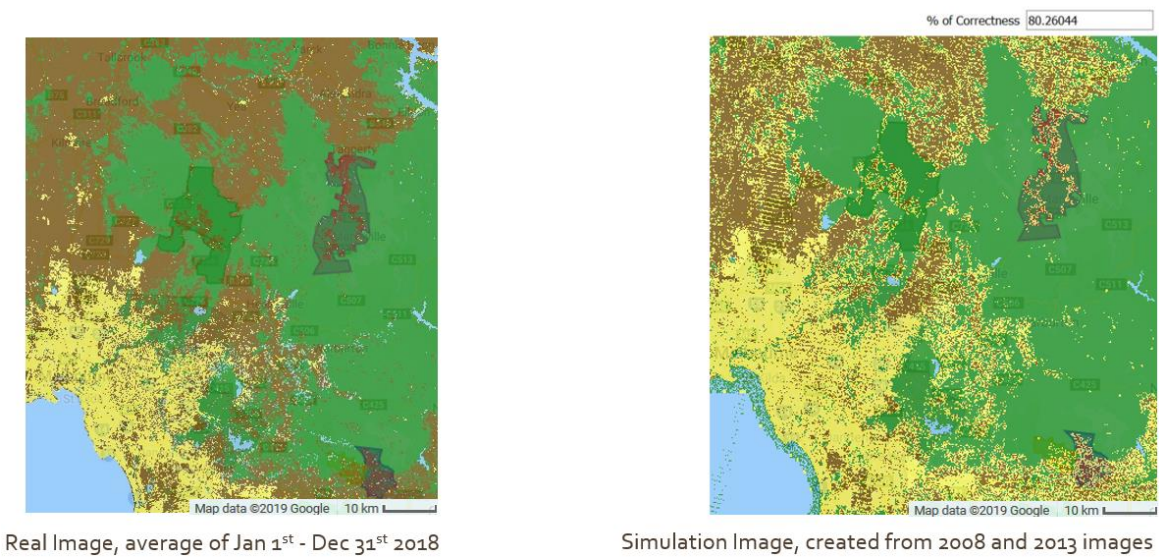


Figure 26. “Real” vs. “Simulated” image in Victoria, comparing classification accuracy.



Figure 27. Result of Simulation predicting landcover classes for (the year) 2030.

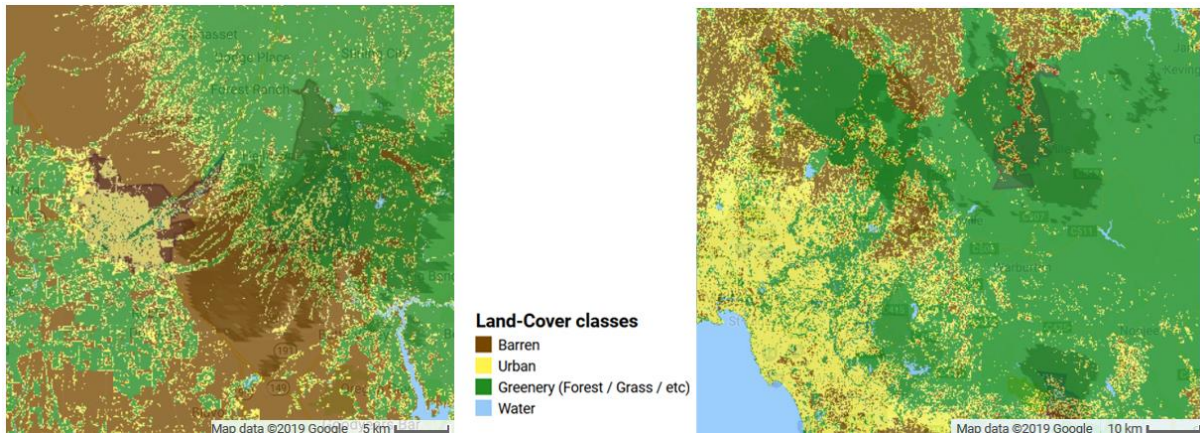


Figure 28. Result of Simulation predicting landcover classes for (the year) 2040.

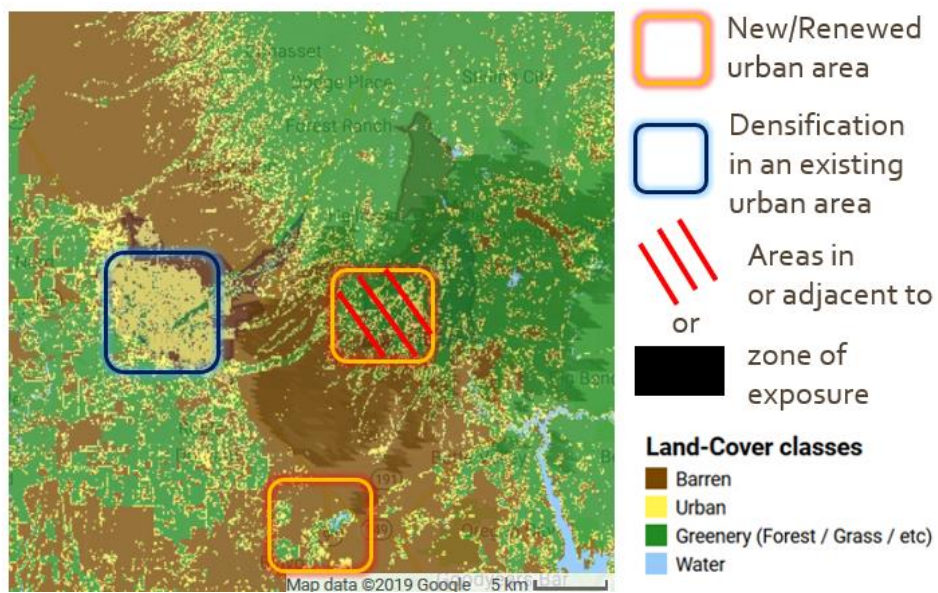


Figure 29. Urban Densification & Creation in the Camp Fires' Zone of Exposure.

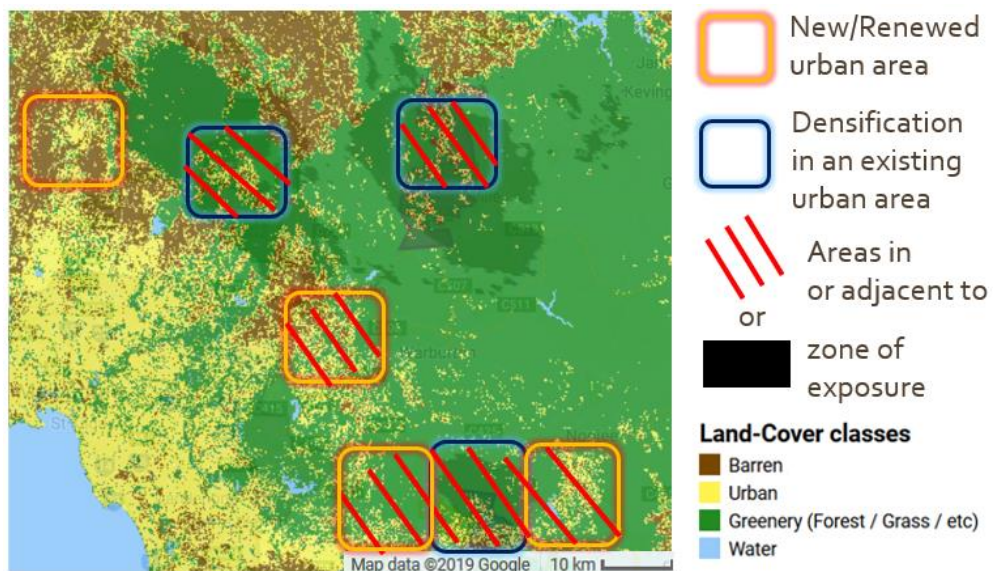


Figure 30. Urban Densification & Creation in the Black Saturday Fires' Zone of Exposure.

Section 3.5. Per-Decade Comparative Environmental Vulnerability Factors | (VA.1) – (VA.4)

Figure 31 shows a survey of the temperature across the study area in California and Victoria. Each area had the temperature taken for a one-year annual average in 2000, 2009 (Victoria), 2010 (California), and 2018. In California, we see average temperature drop from 15 Celsius (C) to 13C on average comparing (a) 2000 to (b) 2010, and then rise to 18C in (c) 2018 – right before the *Camp Fire* occurred. Victoria sees the average temperature sharply rise between (d) 2000 and (e) 2009 (when the fires occurred) from 14C to 23C, then return to approximately the same 14C in (f) 2018 as it was in 2000. Overall, we notice that California sees a gradual rise in temperatures, while Victoria tends to keep a stable temperature around 14C, except for in 2009 when a sudden increase in temperature had occurred. In both cases, it is quite likely that this rise in temperature (whether gradual or sudden) would have contributed to making each area much more vulnerable to a wildfire event like the ones that occurred. In the future, if this trend is to continue, California should monitor its warming, and Victoria would want to watch out for other spikes in temperature.

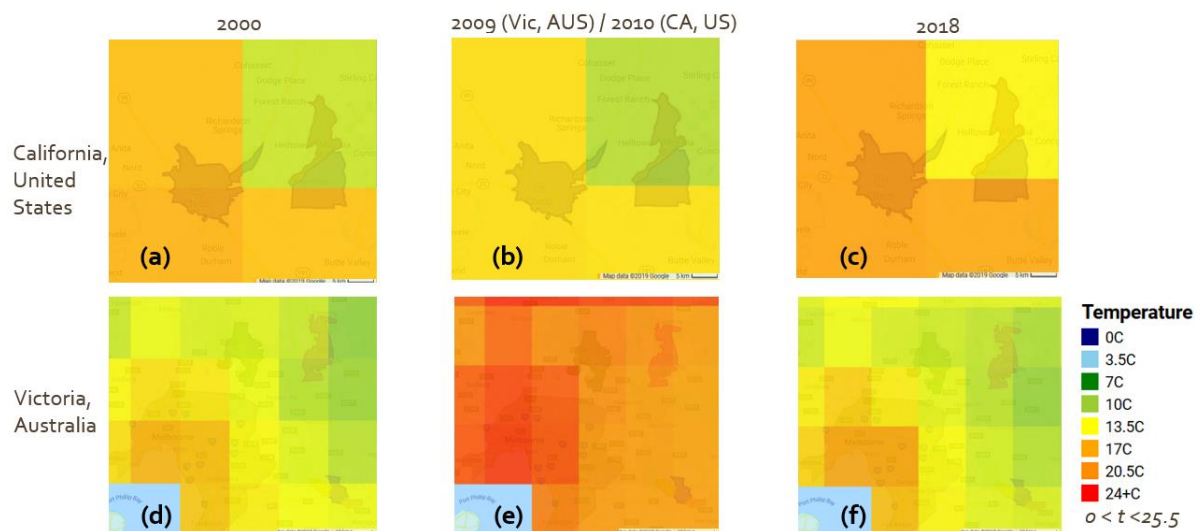


Figure 31. Per-decade comparison of temperature in California and Victoria, 2000-2018.

Figure 32 shows the changes in the soil moisture (as measured at the surface of the soil) for California and Victoria. In California, we see that the soil moisture in the WUI regions (right-half) is clearly and significantly worse than that of the nearby larger city (left-half), probably because of the sloped landscape of the WUI and the flatter landscape present in the city. Over time, we see that California has an unchanging amount of soil moisture from (a) 2000 to (b) 2010, around 25 liters per cubic meter (l/m^3) in the larger cities and about 21 l/m^3 in the WUI communities. Then, in (c) 2018 we see a rapid decrease towards 17 l/m^3 in the WUI communities and the northern-half of the larger city, and even a drop from 28 to 23 l/m^3 in the southern half of the larger city. In Victoria, we see a similar trend to what we saw with the temperature – a more constant value at 2000 and 2018, with a sudden change of value in 2009. In (d) 2000, we see that the soil moisture was rather high – in the WUI this was 23-26 l/m^3 in the Kinglake region, 28-30 l/m^3 in the Marysville region, and around 27 l/m^3 in the Labertouche region, while varying between 25-31 l/m^3 in Melbourne metropolitan regions. Comparatively, (e) 2009 shows a sharp decrease across all regions of the *Black Saturday Fires* study area – in Kinglake and Marysville the soil moisture was around 14.5 – 18 l/m^3 (a drop of about 10 l/m^3) Labertouche saw 18 – 21 l/m^3 (a drop of about 7 l/m^3), and Melbourne’s soil moisture was around 21 – 25 l/m^3 (a drop of approximately 8 l/m^3). Currently, (f) 2018 shows values about 2 l/m^3 lower than 2000, but at least 5 l/m^3 higher than soil moisture values from 2009. If this trend were to continue, California should consider the previous decades’ gradual decrease, and Victoria should exercise caution in years with sudden declines in soil moisture.

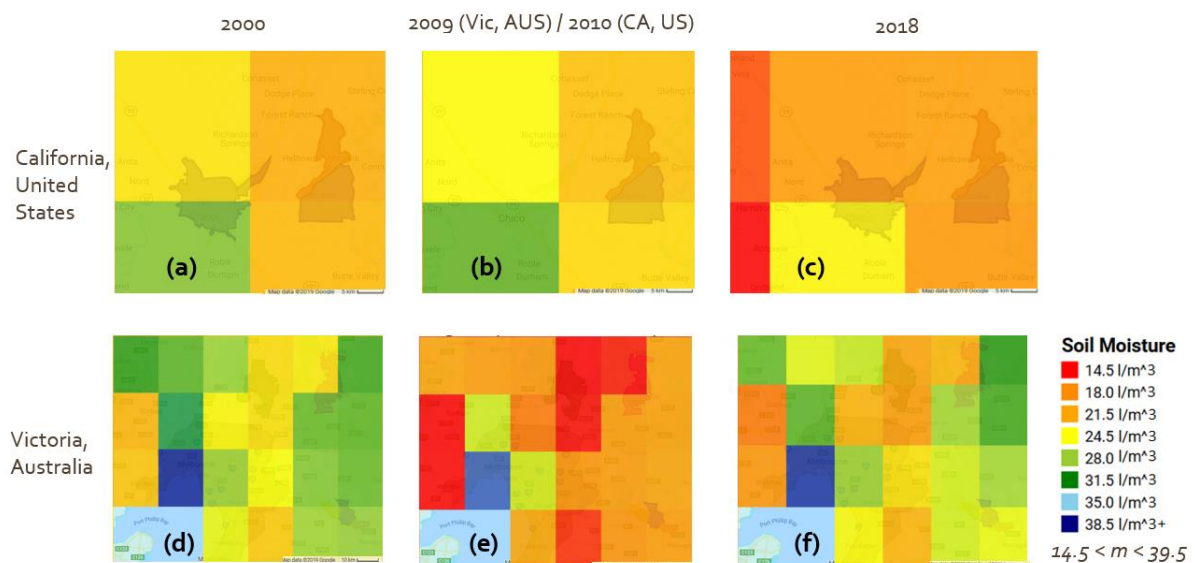


Figure 32. Per-decade comparison of soil moisture in California and Victoria, 2000-2018.

Figure 33 shows that in both regions, the wind's direction has a substantial influence on if a fire will (or will not) spread in that same direction. While there is a remote sensing satellite “NOAA RTMA” measuring wind directionality for the continental United States, there was (and still is) no other satellite which measures Australia's (or anywhere else in the world's) wind directionality. Hence, we see that (c) makes use of the Australian federal Bureau of Meteorology's wind map instead. For (a), we see that on November 8th, the average wind direction during the day was to the south-west in the WUI communities (near Paradise and other towns) with a wind blowing to the East in most the remainder of the study area. Surprisingly, the nearby large city of Chico has a wind also blowing in the west, perhaps an effect of embers of the fire. More curious, as shown in (b) while the fire followed the wind's direction in the WUI regions, the fire stops at the boundary with the east wind. While not depicted here, this counter-direction wind is not present on the second day, and the fire continues to spread into Chico on that day (but successful firefighting efforts move the fire out of the large city and the inhabited WUI communities by the third day). In Victoria, a similar trend may be observed – (c) shows that there are two directions amongst the winds present – an ocean wind blowing to the Northeast and an on-land wind blowing into the Southeast. Further, the wind direction curves on the map indicate that the two wind fronts collide in a near-diagonal line around the outskirts of the Melbourne metropolis. As (d) shows, all the fires in the WUI on the first day of the *Black Saturday Fires* on February 7th follow a southeastern progression, matching the winds on that side of the divide. The RTMA satellite over the United States only began its service relatively recently, and we've yet to see other satellites launched for the rest of the world, but monitoring wind direction averages on annual or larger scales may show which areas have a higher vulnerability to wildfire.

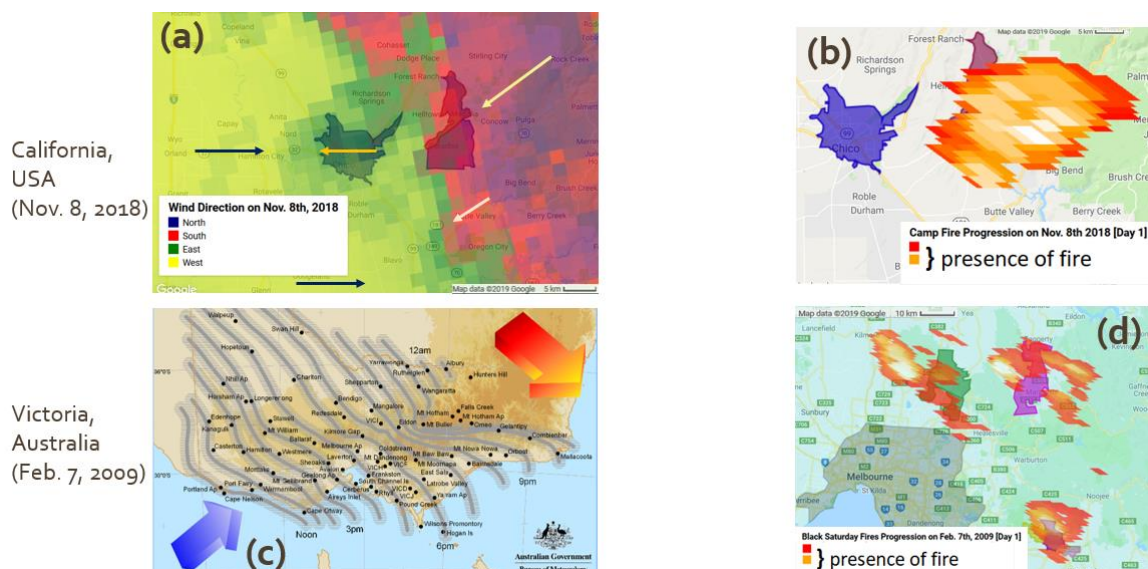


Figure 33. Comparison of wind direction and fire progression for the first day of each fire. (Top shows Camp Fire in California, bottom shows Black Saturday Fires in Victoria).

Figure 34 shows the annual cumulative rainfall in California and Victoria, for 2000, 2009/2010, and 2018, with only the period before the fire being reflected for years when there was a wildfire. For each decade, we can see some apparent changes in the amounts. To begin with (a) shows a uniform 600-700 millimeters (mm) throughout the study area in California in 2000, which (b) in 2010 increases to 1200-1500 mm throughout the area (with the WUI receiving slightly more rain). (c) Before the fire in 2018, we see that WUI region which burned during the fires is receiving more rain (closer to 700 mm) than the nearby city region (only about 500 mm) – yet the fire still burned through the WUI. In (d) 2000, we see that there was around 750 – 900 mm of rain in most the study region of Victoria, with the region from southern Marysville to Labertouche receiving 1000 – 1315 mm of rain. (e) Before the fire in 2009, we see that there was no rain in most parts of Victoria (and no more than 15 mm in the wetter Marysville-Labertouche region), which may have contributed to the dry soil moisture of that year. Currently, in (f) 2018, we see that the wetter region of the study area in Victoria received 700 – 800 mm while the drier areas have only received 400 – 600 mm through the whole year. While rain seems to have some correlation with the soil moisture values, the rain itself (as evidenced by the fact that fires can burn in the areas which received more rain and not in the areas which received less) is probably not a direct vulnerability factor. Still, considering its influence on the other factors, it is important to find the cumulative rainfall's trend in the last couple decades: in California, we generally see dry years with occasional rain, and in Victoria, we have seen a gradual drying with the potential for no rain at the beginning of the year (which is their summer). While probably not a direct vulnerability factor, monitoring cumulative rainfall will likely continue to be important in deciding which areas have the highest risk for wildfire damage.

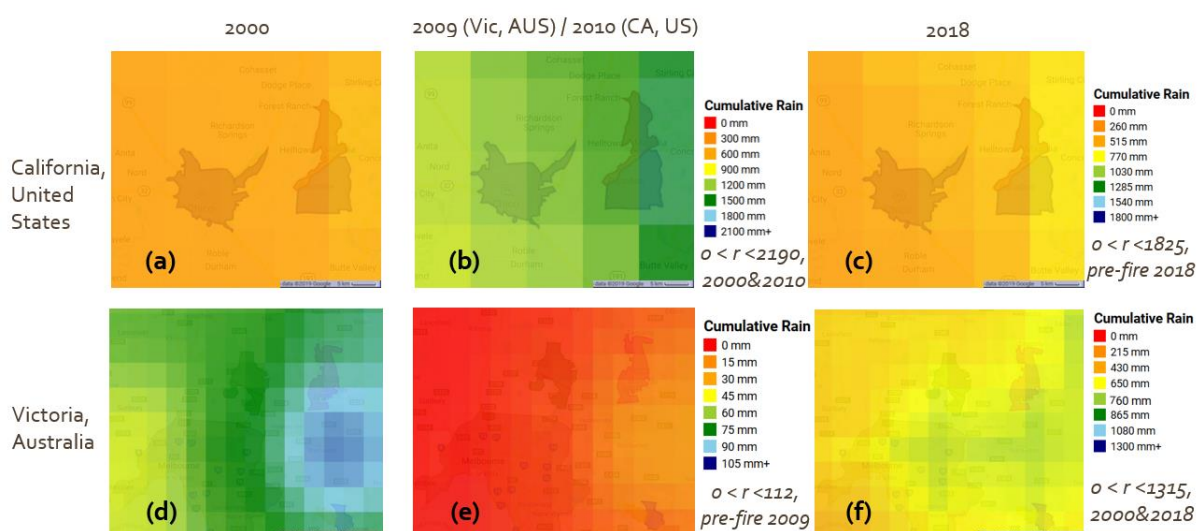


Figure 34. Per-decade comparison of rainfall in California and Victoria, 2000-2018.

Section 3.6. Social Vulnerability: Present-Day Fire Station Locations | (VA.5)

Figure 35 shows the current location of fire stations, represented as an orange dot for each station in service (current as of mid-2019). The green dot on the left image is a fire station that was burned down in Paradise, California during the Camp Fire and now no longer exists. Not counting that one station, there are a total of 32 fire stations operating within the *Camp Fire* study area and 85 stations operating within the *Black Saturday Fires* study area. Further, not counting the stations in Chico (nearby larger city) means that there are 25 stations in the WUI communities, and a similar count to exclude Melbourne's leaves 29 stations within WUI towns. As the *Camp Fire* study area is 6000 square kilometers (sq. km.) and the *Black Saturday Fires* one is 12000 sq. km., this means there are (on average) about ~200 sq. km. (~240 sq. km. in the WUI) per station in California's study area and ~141.77 sq. km. (~413.80 sq. km. in the WUI) per station in Victoria's area.

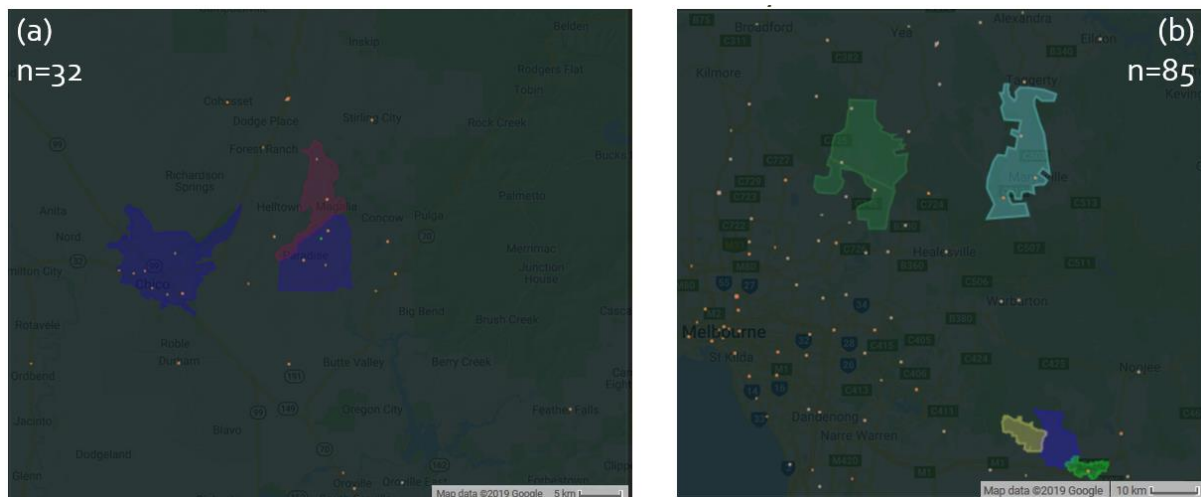


Figure 35. Location maps of fire stations in California and Victoria's study areas.

Further, if we consider the average speed and suggested response time, we can work out how much area each fire station can cover (assuming response via fire truck vehicle) within the recommended time to respond. Comparing this to the fire station density should give us an idea if there are enough fire stations in each study area. In California, the Vehicle Code Title Law 22362 (1970) dictates that the presumed speed limit is 25 miles (40 km) per hour in residential and business zones. In Victoria, their Road Safety Rules (2017) state that rural and suburban zones are to be traversed at less than 50 km per hour. Further, the National Fire Protection Association says that all firefighters in the US should aim to respond within 14 minutes for rural area fires (NFPA, 2010) and Victoria's Country Fire Authority aims for an average of 15 minutes (10-20 minutes) to respond to rural fires (CFA, 2017).

Taking these values into account, we see that at 40 km/hr you can travel a radius of 9.3 km within 14 minutes, so any single fire station within the California study area should be able to cover an average total ~273.67 sq. km. to be within an acceptable standard. Both the WUI and overall fire station density are agreeable to this, as both values are less than the ~274 sq. km. threshold. For Victoria, a similar calculation reveals a travel radius of 12.5 km within 15 minutes, so any fire station should be able to cover an average ~490.87 sq. km. area within their acceptable standard. Again, both overall and WUI fire station density are currently adequate. Table 8 summarizes these results.

However, as areas in the WUI continue to develop, the response time standard will lower (5 min. 20 sec. is the most stringent US standard, 8 min for CFA standards) which would eventually require an increase in the number of fire stations. However, as the laws and situation currently are, the social vulnerability of having enough fire stations for these WUI communities is effectively mitigated.

Table 8. Fire Response Time Standards, Lawful Maximum Driving Speed, and Effective Response-Ready Area for each Study Area

	California	Victoria
[a] Fire Response Time (<i>min</i>)	14	15
[b] Lawful Max Driving Speed (<i>km / hr</i>)	40	50
[c] Effective Ready-to-Respond Area (<i>sq. km.</i>)	273.67	490.87
[d] Fire Station Density in WUI (<i>sq. km. / station</i>)	~240	~413.80
Vulnerability mitigated? (<i>Boolean, is [c] > [d]?</i>)	Yes	Yes

Section 4. Conclusion and Future Work

Section 4.1. Conclusion

In closing, this study has determined the risk factors that affect damage to WUI regions from wildfires, based on the hazard, exposure, and vulnerability model of risk. In doing this, this paper measured hazard factors of the average speed of fire spread, burned area totals, and burn severity for each of the *Camp Fire* and *Black Saturday Fires*. This thesis also utilizes a classifier algorithm separating landcover into four types: barren/burnt, urban, greenery, and water-covered and created a simulation that showed future landcover classification, in 2030 and 2040. By overlaying the 2040 image for each region with the exposure as measured from the burned area (hazard analysis), we see that newly created urban and urban densification areas is relatively low and unchanging within and neighboring the California study area's zone of exposure. In Victoria, we determined that these urban areas are more prone to exposure, due to a significant quantity of new urbanization within and adjacent to existing WUI communities and metropolis. However, there was a limitation in the algorithm giving too much signal response for urban areas, creating small dotted noise. While these were not counted as urban regions, future work is necessary to clean it.

The study also considered the effect of various environmental vulnerability factors - including temperature, soil moisture, wind direction, and precipitation. To begin with, we noted that precipitation likely affected the other vulnerability variables, but was not itself one. In California, we saw that the environmental vulnerabilities showed more slight effect for temperature and soil moisture, but a much clearer effect from the wind direction. Currently (in 2018), the California study area shows gradually rising temperature, decreasing soil moisture, and a fixed amount of rain (relative 2000). In Victoria, the environmental vulnerabilities were apparent for all factors (including rainfall) when measured before the 2009 fire and compared to previous imagery from 2000. Relative 2000, we at-present (in 2018) see a similar temperature but slightly decreased soil moisture and rainfall in the Victoria study area. Despite showing one of the strongest correlations to wildfire, a significant limitation of this section was that wind direction is a relatively new satellite sensing product not available outside the United States. The future development of such a product would greatly benefit this area of wildfire vulnerability research.

Finally, a study was conducted on the social vulnerability of wildfire based on the availability and density of fire stations. The fire station density was calculated and derived so that there is a fire station every 240 sq. km. (California) or 413.8 sq. km. (Victoria) in the WUI regions, with slightly lower values of area for each station over the entire study region.

We then used average lawful vehicular driving speed and recommended standards for fire response time, and calculated on average what each fire station could respond to “on-time.” In California, this was an area of 273.67 sq. km. and in Victoria, this was 490.87 sq. km. Comparing these values with the average density of fire stations showed that there are enough. However, assuming novel urban creation, expansion, and densification, it is likely that more stations will need to be built in the future to keep susceptibility to wildfire low. While these nearby WUI fire stations are an essential measure of containing vulnerability by being the first responders to preventing wildfire spread, the main weakness is that they are not going to be the only responders for higher intensity, longer-timescale fire. Perhaps a future study would consider the street plans, building construction material, or height of buildings as additional social vulnerability factors.

Finally, it would be beneficial for the results of this study to translate into some advice to be given to city and emergency planners. In what this paper discovered, watching 1-year and 5-year averages for wind directionality might help to show which direction(s) to be avoided when considering developing new land for housing. Similarly, while building homes following the advice of Caggiano et al. (2016) and leave at least 30m buffer from vegetation around all houses, commercial centers, and other artificial developments, to prevent the rapid spread of wildfire via embers. Perhaps the expansion of the town itself could also be limited, halting growth in the area exposed areas which need to be defended from wildfires. On the other side of that, if the town becomes denser, expands, or a new urban area is created then there need to be enough fire stations built and/or there needs to be an improvement in the response time – 15 minutes probably feels like a lot when you are watching your house (and all the other homes in the neighborhood) burn down. Finally, an unusual thing to observe was that the initial portion of the Camp Fire happened during a heavy rainstorm – having a wet climate is not protection from the damaging effects of wildfire on WUI communities.

Section 4.2. Future Work

With the discussion of the limitations in the previous subsection, it is best to consider what projects could be undertaken to find further results, improve accuracy, or otherwise derivate on this research.

For example, as mentioned before the simulations created in this project were noisy and over-expressive of the urban signal. This could probably be fixed in one of a couple of ways – one is where more generations are run for the neural network; the other is where the neural network is operated in the same configuration many more times and an average

image of all results is considered (hopefully smoothing out any outliers). In the former method, Suresh et al. (2010) have shown in the machine learning field of study that there is a discrete number of generations that acts as the optimal training threshold – anything after this and the model is less accurate, or *over-trained*. The latter method makes use of average smoothing and outlier rejection methods of statistics, where the data these methods are applied to is represented in the form of images. While potentially much more time-intensive than the former process, the collection of many images gives potential to be much more accurate – as MOLUSCE runs every simulation trial at a different, randomized weight.

The limitations found during gathering results for vulnerability analysis also need addressing. In addition to the issues and ideas listed previously, it is difficult to analyze the correlative effect of 18 years' worth of discrete data points, let alone present the information comprehensively. Google Earth Engine does a good job of displaying the image as a map overlay for separate “snippets” of time (which in this case is any single year listed in Table 2), but had a line chart been created then this study could have given continuous data which would allow interval analysis, and show potentially hidden data, from the years not analyzed.

Mostly separate from the limitations, some ideas can be thought up of for further work to this study. As mentioned in the introduction, the top 20 ranked wildfire human deaths and structural damage incidents, since 2000, also include two in Greece (one in 2007 and the other in 2018). Including the Eastern Russia wildfire in 2010 (at rank 25) as well, would all be great case studies to expand this study. Further, it should theoretically be possible to use the same MOLUSCE simulation software and simulated landcover images and combine this with all the environmental vulnerability factors and fire-progression hazard-factors to model the spread of the wildfires in these future urban areas. On that note, the software algorithm currently being used for the CA-ANN, MOLUSCE has fallen out of active development and is not (a) compatible with current versions of QGIS software package and (b) does not support efficient processing through the distribution of resources. Finally, the current version of all this study's algorithms depends solely on organizing table information in Fusion Tables (a Google research product), which will be sunsetting at the end of 2019. The (assumed) launch of Google Earth Engine Apps (with its ability for the public to view it) would present an excellent opportunity to modernize all the code and host the GIS risk maps on a website, so that the public (see Appendix A) may access and benefit from the data. Improving technological ability, cost-effectiveness, and better-written algorithms should make these additional studies more feasible and attractive to carry out.

Appendix A. Communication of Data with the Public

This thesis study attempts to make available all data, and more importantly, the programming scripts and assets which created it, to members of the public for their studies and discussions with disaster-management and citizen science groups. The following subsections of this appendix offer detailed information about each platform.

Section A.1. Introduction to and Accessing Data from GitHub

GitHub is a platform for software developers to store, version, and open-source their projects in units called “repositories.” GitHub is a combination of “git” - the system many developers use for code versioning while building their program and “hub” – a place where many like-minded developers can meet and code together. “Git” has been around since 2005 for the Linux kernel and operating system and GitHub has been operating since 2008, with a dedicated Japan office opened in 2015. The platform allows for the upload, both to the public and for private use (yourself or organizations of people), of programming code, binary files, shell scripts, documents, licenses, etc. to (as of late 2018) over 100 million repositories. The data for this thesis is publicly available in the form of JavaScript programming code and other supporting files. However, it does not include Google Earth Engine (GEE) runtime tools (as the licensing nor access is available). Hence, one cannot currently (in mid-2019) make edits and receive the outputs of the programming code written without access to GEE. This limitation is acceptable – having data available now opens the way for derivative projects when GEE becomes a more openly-accessible product.

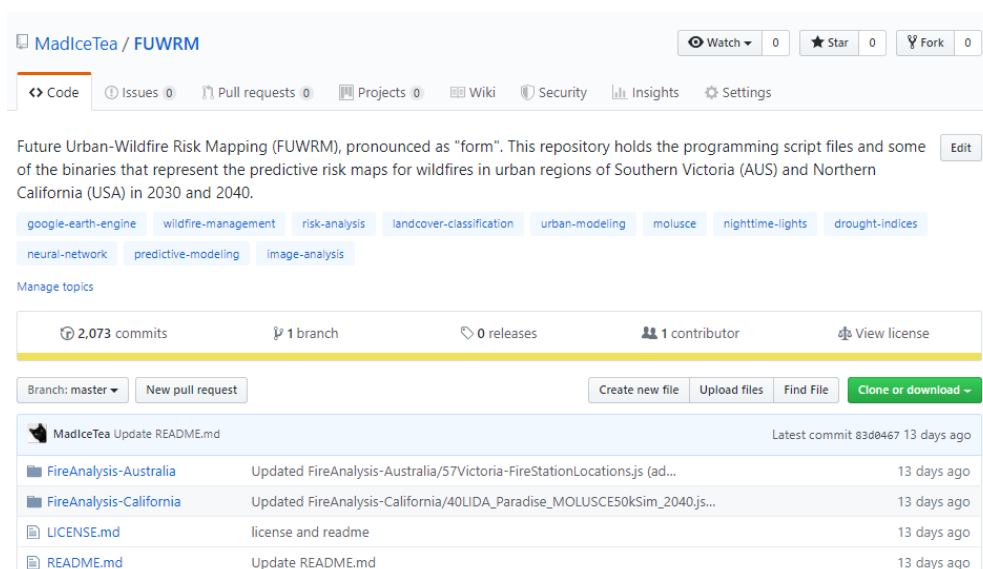


Figure 36. An interim screenshot of the GitHub repository for this project.

In the future, having the code available through GitHub will lead to potential collaborations, bugfixes, and incentive to keep all the algorithms current and accurate. It should also bring awareness to disaster management for other natural phenomena amongst an informed public and academic researchers.

A repository of Google Earth Engine programming code on GitHub can be accessed here: **github.com/MadIceTea/FUWRM**.

Section A.2. Introduction to and Accessing Data from Google Earth Engine

Google Earth Engine (GEE) is a platform for the large-scale “big data” analysis of satellite and remote sensing data. Commands can be issued against a parallel processing server in the form of programming language algorithms, either written in “JavaScript” or “Python.” Only JavaScript was used to make the programs for this thesis. The platform requires an initial signup process to access, where we agree to use GEE for mostly non-commercial purposes. Acceptance is the prerogative of Google’s engineers, but access is a prerequisite to run the programs which query regularly updated satellite data repositories against a google maps image of the region of interest.

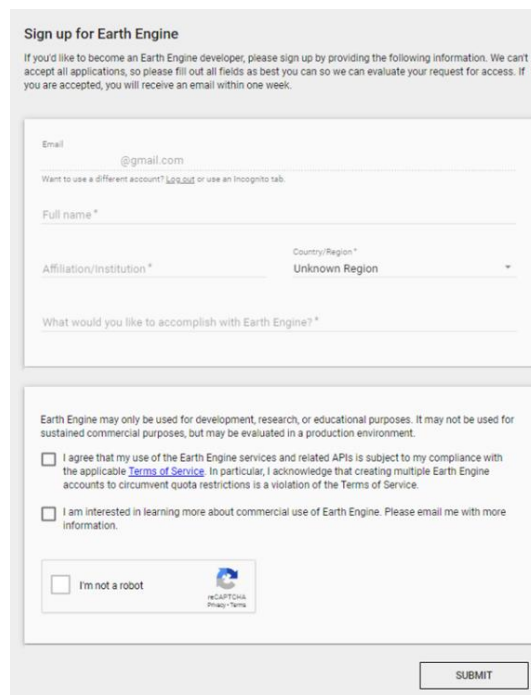
The image shows a web form titled "Sign up for Earth Engine". It includes a paragraph of introductory text, followed by input fields for "Email", "Full name", "Affiliation/Institution", and "Country/Region". Below these is a text area for "What would you like to accomplish with Earth Engine?". A section of terms and conditions follows, with two checkboxes: "I agree that my use of the Earth Engine services and related APIs is subject to my compliance with the applicable Terms of Service" and "I am interested in learning more about commercial use of Earth Engine. Please email me with more information.". At the bottom left is a CAPTCHA checkbox labeled "I'm not a robot" with a CAPTCHA logo. A "SUBMIT" button is at the bottom right.

Figure 37. Signup form for Google Earth Engine (as of mid-2019).

In this study, Google Earth Engine repositories are used to track fire progression, landcover, wind direction in the United States, and drought index – to name a few.

A Google Earth Engine programming code repository used in this thesis is available: **code.earthengine.google.com/?accept_repo=users/GEE_Alex/RiskAnalysis_Fire-Urban**

Google stores code created within repositories in the same “git” format as previously mentioned (in section A.1) which makes it easy for code migration to GitHub.

I export (so-called “pull”) the programs, complete with the historical changes that each save brought to the project’s collection of programming codes, and then re-import into the GitHub repository via “clone” commands (a programmer’s equivalent to copy-and-paste), and upload via “push” command. This process ensures algorithms written in the invite-only GEE program is available to be inspected and transformed by others interested in similar projects around the world and for all other forms of disaster-causing natural phenomena.

Google is also piloting a new experimental program called Google Earth Engine applications (“Earth Engine App”), which allows the public to view the results of single programs in Earth Engine repositories. Apps might be a potential vector for future work in sharing results of this study’s work in an easy-to-comprehend demonstration to the public. Currently, a significant limitation of App is the lack of viewable source-code. With further encourage others to conduct similar research.

A sample Google Earth Engine App, based on this study’s investigation of cumulative precipitation in Victoria in 2000, is available at the following link:

[gee_alex.users.earthengine.app](https://www.earthengineapps.com/gee_alex.users.earthengine.app)

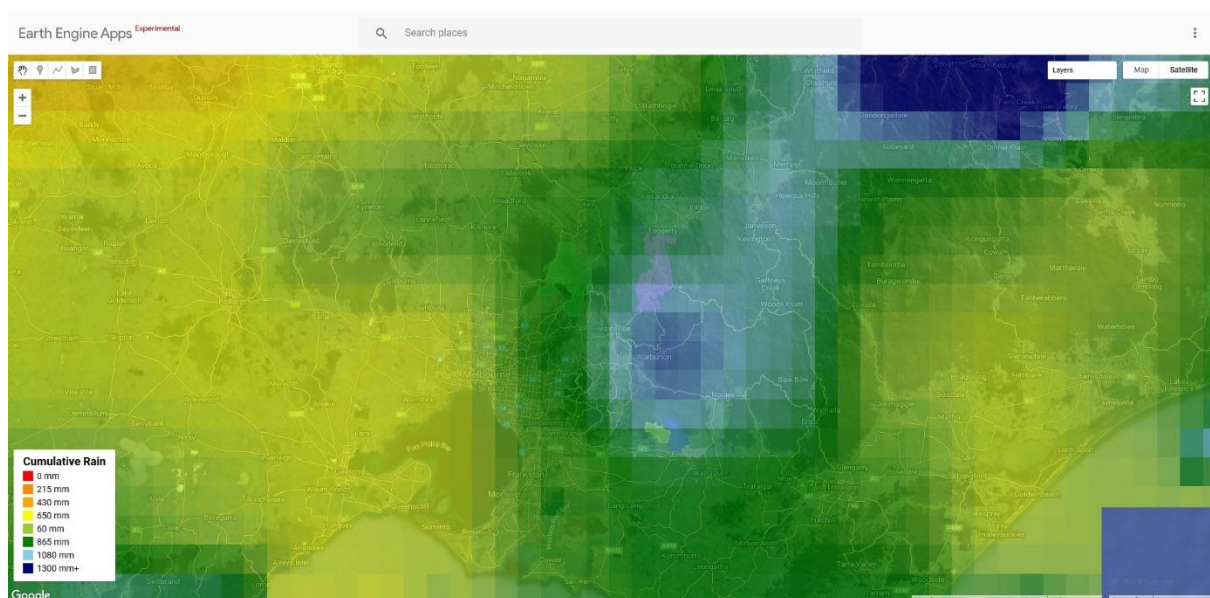


Figure 38. Sample Earth Engine App created as a proof-of-concept. The map shows cumulative rainfall over a portion of southern Victoria for (the year) 2000.

References

- [1]. Aitchison, A. (2011, January 23). The Google Maps / Bing Maps Spherical Mercator Projection. Retrieved from <https://alastaira.wordpress.com/2011/01/23/the-google-maps-bing-maps-spherical-mercator-projection/>
- [2]. Arroyo, L. A., Pascual, C., & Manzanera, J. A. (2008, September 5). Fire models and methods to map fuel types: The role of remote sensing. *Forest Ecology and Management*, 256(6), 1239-1252. doi:10.1016/j.foreco.2008.06.048
- [3]. Bettinger, P., Boston, K., Siry, J. P., & Grebner, D. L. (2017). Geographic Information and Land Classification in Support of Forest Planning. In *Forest Management and Planning* (pp. 65-85). Elsevier Science Publishing Co.
- [4]. Breiman, L., Friedman, J. H., Olshen, R. A., & Stone, C. J. (1984). Classification and Regression Trees. doi:10.1201/9781315139470
- [5]. Caggiano, M. D., Tinkham, W. T., Hoffman, C., Cheng, A. S., & Hawbaker, T. J. (2016, October). High resolution mapping of development in the wildland-urban interface using object-based image extraction. *Heliyon*, 2(10). doi:10.1016/j.heliyon.2016.e00174
- [6]. CAL FIRE. (2019, July 9). Welcome to Incident | Camp Fire. Retrieved from <https://www.fire.ca.gov/incident/?incident=75d4fe80-f18a-4a4a-9a37-4b564c5f6014#incident-contacts>
- [7]. Calkin, D. E., Cohen, J. D., Finney, M. A., & Thompson, M. P. (2014, January 14). How risk management can prevent future wildfire disasters in the wildland-urban interface. *Proceedings of the National Academy of Sciences*, 111(2), 746-751. doi:10.1073/pnas.1315088111
- [8]. CIESIN, Columbia University. (2017, December). Gridded Population of the World (GPW), v4 | SEDAC. Retrieved from <https://sedac.ciesin.columbia.edu/data/collection/gpw-v4>
- [9]. Clark, T. L., Coen, J., & Latham, D. (2004, April 8). Description of a coupled atmosphere - fire model. *International Journal of Wildland Fire*, 13(1), 49-63. doi:10.1071/wf03043
- [10]. Colac Otway Shire, Thompson, H., Fong, G., Corbett, J., Fong, B., Cox, A., . . . Briody, C. (2011, March 11). 4.3 Hazard, Exposure, Vulnerability and Resilience. Retrieved from <http://memp.colacotway.vic.gov.au/cho1s04s03.php>
- [11]. Department of Motor Vehicles, State of California. (1970). Speed Laws | Generally [22348 - 22366]. Retrieved from https://leginfo.legislature.ca.gov/faces/codes_displaySection.xhtml?lawCode=VEH§ionNum=22362.
- [12]. DeWitt, M., Johnston, R., Gibson, D., Scott, L., & Software Engineers. (2018, September 28). Share your analyses using Earth Engine Apps - Google Earth and Earth Engine. Retrieved from <https://medium.com/google-earth/share-your-analyses-using-earth-engine-apps-1ac29939903f>

- [13]. Doyle, J. (2015, March 19). Emergency Service Response Times. Retrieved from <https://www.audit.vic.gov.au/report/emergency-service-response-times?section=31488--2-relevant-measures-and-targets>
- [14]. Elvidge, C. D., Baugh, K. E., Kihn, E. A., Kroehl, H. W., Davis, E. R., & Davis, C. W. (1997). Relation between satellite observed visible-near infrared emissions, population, economic activity and electric power consumption. *International Journal of Remote Sensing*, 18(6), 1373-1379. doi:10.1080/014311697218485
- [15]. Ferris, E., Petz, D., & Stark, C. (2013, March 1). It Only Takes a Spark: The Hazards of Wildfires Chapter 3 of The Year of Recurring Disasters: A Review of Natural Disasters in 2012. Retrieved from <https://www.brookings.edu/research/it-only-takes-a-spark-the-hazards-of-wildfireschapter-3-of-the-year-of-recurring-disasters-a-review-of-natural-disasters-in-2012/>
- [16]. Giglio, L., Boschetti, L., Roy, D. P., Humber, M. L., & Justice, C. O. (2018, November). The Collection 6 MODIS burned area mapping algorithm and product. *Remote Sensing of Environment*, 217, 72-85. doi:10.1016/j.rse.2018.08.005
- [17]. Giglio, L., Randerson, J. T., Werf, G. R., Kasibhatla, P. S., Collatz, G. J., Morton, D. C., & Defries, R. S. (2010, March 1). Assessing variability and long-term trends in burned area by merging multiple satellite fire products. *Biogeosciences*, 7(3), 1171-1186. doi:10.5194/bg-7-1171-2010
- [18]. Gorelick, N., Hancher, M., Dixon, M., Ilyushchenko, S., Thau, D., & Moore, R. (2017, December 1). Google Earth Engine: Planetary-scale geospatial analysis for everyone. *Remote Sensing of Environment*, 202, 18-27. doi:10.1016/j.rse.2017.06.031
- [19]. Government of Australia. (2006, September). Australian Coastal outline and Landmass with State boundaries. Retrieved from http://data.daff.gov.au/anrdl/metadata_files/pa_nsaasr9nnd_02211a04.xml
- [20]. Government of Victoria, Australia. (2019, February 28). Speed limit. Retrieved from <https://www.vicroads.vic.gov.au/safety-and-road-rules/road-rules/a-to-z-of-road-rules/speed-limits>
- [21]. Horie, D. (2015, June 04). Announcing GitHub Japan. Retrieved from <https://github.blog/2015-06-04-announcing-github-japan/>
- [22]. Key, C. H., & Benson, N. C. (2006). *FIREMON: Fire effects monitoring and inventory system* (pp. 37-38, Tech. No. RMRS-GTR-164-C). USDA Forest Service.
- [23]. Koordinates, & California, S. (2018, September 5). California Counties. Retrieved from <https://koordinates.com/layer/96021-california-counties/>
- [24]. Kottek, M., Grieser, J., Beck, C., Rudolf, B., & Rubel, F. (2006, April 10). World Map of the Köppen-Geiger climate classification updated. *Meteorologische Zeitschrift*, 15(3), 260-261. doi:10.1127/0941-2948/2006/0130
- [25]. Levin, N., & Heimowitz, A. (2012, November). Mapping spatial and temporal patterns of Mediterranean wildfires from MODIS. *Remote Sensing of Environment*, 126, 12-26. doi:10.1016/j.rse.2012.08.003

- [26]. Lillesand, T. M., Kiefer, R. W., & Chipman, J. W. (2015). Chapter 7. Digital Image Analysis. In *Remote sensing and image interpretation* (pp. 538-546). John Wiley & Sons.
- [27]. Megahed, Y., Cabral, P., Silva, J., & Caetano, M. (2015, September 14). Land Cover Mapping Analysis and Urban Growth Modelling Using Remote Sensing Techniques in Greater Cairo Region—Egypt. *ISPRS International Journal of Geo-Information*, 4(3), 1750-1769. doi:10.3390/ijgi4031750
- [28]. Michael, Y., Lensky, I., Brenner, S., Tchetchik, A., Tessler, N., & Helman, D. (2018, September 16). Economic Assessment of Fire Damage to Urban Forest in the Wildland–Urban Interface Using Planet Satellites Constellation Images. *Remote Sensing*, 10(9), 1479. doi:10.3390/rs10091479
- [29]. Miller, J. D., & Thode, A. E. (2007, July). Quantifying burn severity in a heterogeneous landscape with a relative version of the delta Normalized Burn Ratio (dNBR). *Remote Sensing of Environment*, 109(1), 66-80. doi:10.1016/j.rse.2006.12.006
- [30]. Ministry of Internal Affairs and Communication, Japan. (2015). View Municipality data | SSDS | Search by areas. Retrieved from <https://www.e-stat.go.jp/en/regional-statistics/ssdsview/municipality>. Created by filtering A1101 dataset.
- [31]. Myint, S. W., & Wang, L. (2006). Multicriteria decision approach for land use land cover change using Markov chain analysis and a cellular automata approach. *Canadian Journal of Remote Sensing*, 32(6), 390-404. doi:10.5589/m06-032
- [32]. Myoung, B., Kim, S., Nghiem, S., Jia, S., Whitney, K., & Kafatos, M. (2018, January 10). Estimating Live Fuel Moisture from MODIS Satellite Data for Wildfire Danger Assessment in Southern California USA. *Remote Sensing*, 10(2), 87. doi:10.3390/rs10010087
- [33]. National Fire Protection Association (NFPA). (2010). NFPA 1720. Retrieved from <https://www.nfpa.org/Codes-and-Standards/ARCHIVED/Safer-Act-Grant/NFPA-1720>
- [34]. Nauslar, N., Abatzoglou, J., & Marsh, P. (2018, June 09). The 2017 North Bay and Southern California Fires: A Case Study. *Fire*, 1(1), 18. doi:10.3390/fire1010018
- [35]. NextGIS, & Asia Air Survey. (2013, November 04). MOLUSCE – quick and convenient analysis of land cover changes. Retrieved from <http://nextgis.com/blog/molusce/>
- [36]. Population Australia. (2018). Melbourne Population 2019. Retrieved from <http://www.population.net.au/melbourne-population/>
- [37]. Radeloff, V. C., Hammer, R. B., Stewart, S. I., Fried, J. S., Holcomb, S. S., & McKeefry, J. F. (2005, June 1). The Wildland–Urban Interface in The United States. *Ecological Applications*, 15(3), 799-805. doi:10.1890/04-1413
- [38]. Radeloff, V. C., Helmers, D. P., Kramer, H. A., Mockrin, M. H., Alexandre, P. M., Bar-Massada, A., . . . Stewart, S. I. (2018, March 27). Rapid growth of the US wildland-urban interface raises wildfire risk. *Proceedings of the National Academy of Sciences*, 115(13), 3314-3319. doi:10.1073/pnas.1718850115

- [39]. Schoennagel, T., Balch, J. K., Brenkert-Smith, H., Dennison, P. E., Harvey, B. J., Krawchuk, M. A., . . . Whitlock, C. (2017, May 2). Adapt to more wildfire in western North American forests as climate changes. *Proceedings of the National Academy of Sciences*, 114(18), 4582-4590. doi:10.1073/pnas.1617464114
- [40]. Smith, A. M., Kolden, C. A., Tinkham, W. T., Talhelm, A. F., Marshall, J. D., Hudak, A. T., . . . Gosz, J. R. (2014, November). Remote sensing the vulnerability of vegetation in natural terrestrial ecosystems. *Remote Sensing of Environment*, 154, 322-337. doi:10.1016/j.rse.2014.03.038
- [41]. Stein, S. M., Menakis, J. P., Carr, M. A., Comas, S. J., Stewart, S. I., Cleveland, H., . . . Radeloff, V. C. (2013). *Wildfire, Wildlands, and People: Understanding and Preparing for Wildfire in the Wildland-Urban Interface* (pp. 01-27, Tech. No. RMRS-GTR-299). U.S. Department of Agriculture, Forest Service, Rocky Mountain Research Station. Retrieved from <https://www.fs.fed.us/openspace/fote/reports/GTR-299.pdf>
- [42]. Stevens, F. R., Gaughan, A. E., Linard, C., & Tatem, A. J. (2015, February 17). Disaggregating Census Data for Population Mapping Using Random Forests with Remotely-Sensed and Ancillary Data. *PLOS One*, 10(2). doi:10.1371/journal.pone.0107042
- [43]. Suresh, S., Dong, K., & Kim, H. (2010, October). A sequential learning algorithm for self-adaptive resource allocation network classifier. *Neurocomputing*, 73(16-18), 3012-3019. doi:10.1016/j.neucom.2010.07.003
- [44]. Syphard, A. D., Radeloff, V. C., Hawbaker, T. J., & Stewart, S. I. (2009, May 15). Conservation Threats Due to Human-Caused Increases in Fire Frequency in Mediterranean-Climate Ecosystems. *Conservation Biology*, 23(3), 758-769. doi:10.1111/j.1523-1739.2009.01223.x
- [45]. Tempfli, K., Huurneman, G., Bakker, W., Janssen, L., Feringa, W., Gieske, A., . . . Horn, J. V. (2009). *Principles of remote sensing: An introductory textbook*. ITC.
- [46]. UN-SPIDER. (2018, December 4). Step by Step: Burn Severity mapping in Google Earth Engine. Retrieved from <http://www.un-spider.org/advisory-support/recommended-practices/recommended-practice-burn-severity/burn-severity-earth-engine>
- [47]. UNOOSA. (3 Dec. 1986). 41/65. Principles Relating to Remote Sensing of the Earth from Outer Space. General Assembly Resolutions, UN, New York. Retrieved from <http://www.unoosa.org/oosa/en/ourwork/spacelaw/principles/remote-sensing-principles.html>
- [48]. Warner, J. (2018, November 8). Thank you for 100 million repositories. Retrieved from <https://github.blog/2018-11-08-100M-repos/>
- [49]. WorldPop. (2018, November 1). *Global High-Resolution Population Denominators Project - Funded by The Bill and Melinda Gates Foundation (OPP1134076)*. doi:10.5258/SOTON/WP00645
- [50]. Yale, K. (2018, November 27). Use California Wildfires as a Chance to Rebuild with Design in Mind. Retrieved from <https://www.interiorsandsources.com/article-details/articleid/22409/title/california-wildfires-rebuild-design>